Investigation of ionosphere response to geomagnetic storms over the propagation paths of very low frequency radio waves

Victor U. J. Nwankwo[1], Jean-Pierre Raulin[2], Dra. Emilia Correia[3], William F. Denig[4], Olanike Akinola[5], Olugbenga Ogunmodimu[6], and Rafael R De Oliveira[7]

[1]Anchor University
[2]CRAAM - Universidade Presbiteriana Mackenzie
[3]Instituto Nacional de Pesquisas Espaciais/CRAAM
[4]Retired
[5]Centre For Atmospheric Research, National Space Research and Development Agency, KSU Campus
[6]Department of Electrical and Electronics Engineering, Manchester Metropolitan University
[7]Universidade Presbiteriana Mackenzie

November 24, 2022

Abstract

We analysed variations in signal metrics and the diurnal amplitude of VLF radiowaves from four propagation paths during intervals of 4 geomagnetic storms on 17, 26 September, 25 October and 1 November 2011. Three propagation paths are located at mid-latitude in the Northern Hemisphere, and one crossing the equatorial ionospheric anomaly (EIA) crests and magnetic equator. Our results show significant reduction in the mean amplitude before sunrise (MBSR), the daytime mean amplitude (DTMA) and the mean amplitude after sunset (MASS) signal strength in majority of the cases analysed. The ratio of the storm day signal-decrease (SDSD) to the total number of points (TNoPs) considered are 0.7692, 0.9231 and 0.6923 for MBSR, DTMA and MASS, respectively, while the respective ratio of storm day signal-increase (SDSI) to the TNoPs are 0.1538, 0.0769 and 0.3846. Of the four propagation paths, the DHO-A118 path (in the mid-latitude European sector) showed the largest decrease especially during strong storms (that are associated with solar particle events (SPEs)). We also observed distinct anomaly (large signal fluctuation) in NAA-ROI propagation path signal in South-American region (Brazil). We further investigated the state of the ionosphere over the VLF radiowaves propagation paths using the total election content (TEC) obtained from multiple stations near the transmitters and receivers, to understand these propagation characteristics. Data showed larger enhancement of electron density profiles near the DHO transmitter and ROI receiver, suggesting the large signal strength decrease and fluctuation may be related to markedly perturbed ionosphere along the DHO-A118 and NAA-ROI propagation paths.

Investigation of ionosphere response to geomagnetic storms over the propagation paths of very low frequency radio waves

Victor U. J. Nwankwo[1,2], Jean-Pierre Raulin[2], Emilia Correia[2,3], William Denig[4], Olanike Akinola[5], Olugbenga Ogunmodimu[6], Rafael R. de Oliveira[2]

[1]Space-APRAWP Laboratory, Dept. of Physics Anchor University, Lagos, Nigeria
[2]Centro de Rádio Astronomia e Astrofísica Mackenzie, Universidade Presbiteriana Mackenzie, São Paulo, Brazil
[3]National Institute for Space Research, Sáo José dos Campos, Brazil
[4]St. Joseph College of Maine, Standish, ME 04084, U.S.A
[5]Centre For Atmospheric Research, National Space Research and Development Agency, KSU Campus, Anyigba, Nigeria.
[6]Manchester Metropolitan University, Manchester M15 6BH, United Kingdom

Key Points:

- Analysis of VLF radiowaves amplitude and TEC from multiple receivers during geomagnetic storms on 17, 26 September, 25 October and 1 November 2011
- Results show significant reduction in signal strength and/or fluctuations following geomagnetic storms
- Results also showed larger enhancement of electron density profiles near transmitter and/or reciever larger decrease/fluctuation

Corresponding author: Victor U. J. Nwankwo, vnwankwo@aul.edu.ng

Abstract

We analysed variations in signal metrics and the diurnal amplitude of VLF radiowaves from four propagation paths during intervals of 4 geomagnetic storms on 17, 26 September, 25 October and 1 November 2011. Three propagation paths are located at mid-latitude in the Northern Hemisphere, and one crossing the equatorial ionospheric anomaly (EIA) crests and magnetic equator. Our results show significant reduction in the mean amplitude before sunrise (MBSR), the daytime mean amplitude (DTMA) and the mean amplitude after sunset (MASS) signal strength in majority of the cases analysed. The ratio of the storm day signal-decrease (SDSD) to the total number of points (TNoPs) considered are 0.7692, 0.9231 and 0.6923 for MBSR, DTMA and MASS, respectively, while the respective ratio of storm day signal-increase (SDSI) to the TNoPs are 0.1538, 0.0769 and 0.3846. Of the four propagation paths, the DHO-A118 path (in the mid-latitude European sector) showed the largest decrease especially during strong storms (that are associated with solar particle events (SPEs)). We also observed distinct anormaly (large signal fluctuation) in NAA-ROI propagation path signal in South-American region (Brazil). We further investigated the state of the ionosphere over the VLF radiowaves propagation paths using the total election content (TEC) obtained from multiple stations near the transmitters and receivers, to understand these propagation characteristics. Data showed larger enhancement of electron density profiles near the DHO transmitter and ROI reciever, suggesting the large signal strength decrease and fluctuation may be related to markedly perturbed ionosphere along the DHO-A118 and NAA-ROI propagation paths.

Plain Language Summary

[enter your Plain Language Summary here or delete this section]

1 Introduction

The ionosphere vary significantly with time and geographic location, and also driven by both short- and long-term changes in solar activity, as well as non-solar phenomena (NGDC, 1994). Solar flares, coronal mass ejections (CMEs), high solar wind streams (HSS) and/or corotating interaction regions (CIRs) drives short-term changes in the ionosphere with a time scale ranging from few minutes to days (depending on the phenomena), while long-term ionospheric changes include those related to solar rotation and solar cycle variation. Studies have also shown that the ionosphere can be affected significantly by phenomena that are not directly related to the Sun such as seasonal variation, planetary tides, thermospheric tides, tropospheric tides, and stratospheric warming [(Beynon & Jones, 1965; V. U. Nwankwo et al., 2016);and references therein]. Changes in the regions of the ionosphere are known to sometimes reflect the distinct forcing mechanisms affecting them (V. U. Nwankwo et al., 2016), and various observational capabilities have been exploited to monitor or study such ionospheric responses (to both solar and non-solar phenomena in different regions of the ionosphere). The use of very low frequency (VLF) radiowaves, in the frequency band between 3 kHz and 30 kHz, remains one of the most effective techniques for probing the lower ionosphere and specifically the dayside D-region which is nominal located between 60 to 95 km (Samanes et al., 2018; Mechtly et al., 1967). The structure of the ionosphere consists of a series of discrete layers of increased plasma density formed as a result of production (ionization) versus loss (recombination and chemistry). The ionospheric E-region and F-region density peaks are located above the D-region near altitudes of 110 km and 250 km, respectively (Chapman, 1931). The plasma density of the dayside D-region is mostly maintained by atmospheric photoionization of nitric oxide (NO) by solar hydrogen Lyman-alpha (Ly-α) radiation at a wavelength of 121.6 nm (Nicolet & Aikin, 1960; Nath & Setty, 1976). Other minor or transient sources include collisional ionization by galactic cosmic rays (GCR) (Ohya et al., 2011) and precipitating charged particles (Kikuch & Evans, 1983) and enhanced levels of photoionization by x-rays in solar flares (Anderson et al., 2020). At night and in the absence of a dominant photoionization source the D-region density is greatly diminished as a result of recombination and merges into the lower E-region. VLF waves can be naturally generated, mostly in atmospheric lightning flashes, and manmade, mostly by military transmitters used for submarine communications. Due to their electromagnetic nature, VLF radiowaves can be transmitted over long distances within the Earth-ionosphere waveguide (EIWG) with relatively low attenuation (Wait, 1960).

In the lower ionospheric D-region prompt but short-lived changes due to solar flare associated bursts in solar extreme ultraviolet, X-ray and relativistic solar particles are usually observed as abrupt shifts in the received amplitude and phase of VLF radiowaves. This propagation characterisics have been used to monitor sudden ionospheric disturbance (SID) [e.g., (Mitra, 1974; Thomson & Clilverd, 2001; McRae & Thomson, 2004; Chakrabarti et al., 2005; Pacini & Raulin, 2006; Raulin et al., 2006; Todoroki et al., 2007; Dahlgren et al., 2011; Abd Rashid et al., 2013; Tan et al., 2014; Berdermann et al., 2018) etc.]. The abrupt shift usually observed in VLF signal parameters is in response to flare-induced sudden increase in atmospheric ionisation rate (often referred to as SID), and consequent increase in electron density and the conductivity of the ionosphere. The lower ionospheric D-region can also be disturbed by geomagnetic storms via energetic particle penetration, which can also affect VLF and extreme low frequency (ELF) radio waves propagation in EIWG (Laštovička, 1996; Kikuch & Evans, 1983). The impact of geomagnetic storms on the ionosphere are more intense but often delayed (especially in the middle- and low-latitude) when compared to the solar flare scenario. There is also a distinction in the observed VLF signatures that are affected by the phenomana because their forcing mechanisms differs in time and development. While flare-induced shift in the signal amplitude and phase (especially in the sunlit hemisphere) are easily detectable and well correlated, storm-induced effects appear to be less pronounced and sometimes show no visible spike (V. U. Nwankwo et al., 2016; V. U. J. Nwankwo, 2016). The causal impact of geomagnetic storms on the D-region is not fully understood. Using a sample size of 7 geomagnetic storms, ranging from moderate to intense, Kumar and Kumar (2014) found that the moderate geomagnetic storms (6) had no impact on the signal strength of VLF transmissions whereas a more intense storm with a Dst of -147 nT did cause a marked decrease in signal strength. The authors noted that their findings are in agreement with early published reports [e.g., (Kleimenova et al., 2004; Peter et al., 2006)].

Monitoring and/or probing ionospheric irregularities using VLF radiowaves is limited to the D region because the wavelengths of this radio spectrum lie between 10 km and 100 km [(V. U. J. Nwankwo et al., 2020) and references therein]. Hence the need for other observational capabilities for regions above the D-region. The upper ionospheric variabilities has been studied using ground-based Global Navigation Satellite System (GNSS) receivers, vertical and oblique high frequency (HF) sounding, atmospheric radar (coherent and incoherent scatter radars) and space-based satellite systems such as Advance Composition Explorer (ACE), Constellation Observing System for Meteorology, Ionosphere and Climate (COSMIC), Defense Meteorological Satellite Program (DMSP), Geostationary Operational Environmental Satellite (GOES) etc. There is a unique relationship between the sounding frequency of HF radio pulses and ionospheric ionisation densities that can reflect it (NGDC, 1994), making it possible to study the E and F regions. The variations in the virtual heights of E and F layers (h'E, h'F1 and h'F2), and their critical frequencies (foE, foF1, and foF2) are measured and scaled from ionograms produced by an ionosonde (NGDC, 1994), as well as the electron density (N_mF2) of F2 ionospheric region [e.g., (Sica & Schunk, 1990; Burešová & Laštovička, 2007; Chuo et al., 2013)]. Measured N_mF2 have been used to estimate the height of the F2 peak, h_mF2 (Sica & Schunk, 1990; Burešová & Laštovička, 2007). Ouattara et al. (2009) showed that almost all of these ionospheric parameters (foF2, foF1, foE, foEs, h'F2, h'E, h'Es) exhibits 11-year solar cycle evolution. Such characteristic indicates their sensitivity to solar activity. A large number of ground-based receivers are usually incorporated into the GNSS network and its component Global Positioning System (GPS) network to derive the total Electron Content (TEC) and other ionospheric parameters (e.g., Electron Density Profiles (EDP) and L-band scintillation) that provide good global coverage and description of the ionospheric state (Komjathy et al., 2005; Verkhoglyadova et al., 2016). Geomagnetic disturbances can affect the diurnal variation of the TEC (e.g., (Adeniyi et al., 2014)), and therefore a good parameter for monitoring space weather impacts on the ionosphere [e.g., (Ho et al., 1998; Ding et al., 2008; Mannucci et al., 2009; Jain et al., 2010; Blagoveshchensky et al., 2018) and many others]. Atmospheric radar has the capability to study large-scale dynamical processes in the magnetosphere-ionosphere (IT) system, such as the evolution of configuration of the convection electric field under changing IMF conditions, and development and global extent of large-scale magnetohydrodynamic (MHD) waves in the IT cavity. By monitoring the backscattered power, spectral width and Doppler velocity of plasma density irregularities in the ionosphere via coherent scatter radar (e.g., SuperDARN, EISCAT) the ionospheric manifestations of solar wind and magnetospheric processes in the ionosphere are studied including convection bursts associated with flux transfer events (FTEs), magnetic impulse events (MIEs) and travelling convection vortices (TCVs) (Chisham et al., 2007; Greenwald et al., 1995; Ruohoniemi & Baker, 1998).

Significant effort has gone into characterizing the D-region and lower E-region using VLF transmissions (Barr et al., 2000). Attenuation of the signal strength and retardation of the phase at the receiver location contain information related to the height (H) and sharpness (β) (Thomson et al., 2017) along the propagation path. Given the vast distances over which VLF transmissions propagate there are many geophysical parameters that should be considered, including latitudinal dependencies (Hildebrand, 1993), diurnal variations (Hargreaves & Roberts, 1962) and seasonal changes (Igarashi et al., 2000) which can affect the D-region and, in turn, VLF propagation. In the present study we investigate changes in signal amplitude of radiowave transmissions made during a series of geomagnetic storms in late 2011, while building on previous work [e.g., (V. U. Nwankwo et al., 2016)]. As the use of any single observational tool/data can be inadequate due to the complex nature and temporal variability of the ionosphere (of the Federal Coordinator for Meteorological Services & Research, 2013), a combination of data from different ground-based and/or space-borne systems has been recommended for proper understanding and characterisation of ionospheric responses (Alfonsi et al., 2008; of the Federal Coordinator for Meteorological Services & Research, 2013). Therefore, this work will (in addition) also combine simultaneously observed VLF variations with GNSS/GPS total electron content (TEC) data (from multiple stations) to probe storm effects as it propagates down to the lower ionosphere from the magnetosphere.

2 Data and method

2.1 VLF amplitude propagation in the Earth-ionosphere waveguide

In this work we will utilised the VLF amplitude data of four propagation paths from three transmitters (DHO38 in Germany, GQD in UK and NAA in USA), received at the SID monitoring station in Southern France of Muret at 43.46° N; 1.33° E (with the AAVSO observer code of A118) and ROI station located in Atibaia, Sao Paulo, Brazil. Three (3) of the propagation paths (i.e DHO-A118, GQD-A118 and NAA-A118) are parallel to magnetic equator at mid latitudes in the Northern Hemisphere, and one (i.e NAA-ROI) crossing both equatorial ionospheric anomaly (EIA) crests (north and south) and the magnetic equator. Figure 1 show the propagation paths for VLF radiowave transmissions from DHO38, GQD and NAA. Details of the propagation paths are provided in table 1.

At some point in the study we will lay more emphasy on VLF radiowaves data acquired on the great circle VLF propagation path between the transmitter station DHO38, located in Rhauderfahn Germany (53.09° N, 7.61° E) and the receiver station A118. The

DHO38 transmitter broadcasts on a frequency of 23.4 kHz with a transmit power of 800 kW. The receiving station, A118, is part of the SID network managed by the American Association of Variable Star Observers (AAVSO). The great circle distance for the DHO-A118 VLF propagation path is 1.27 Megameters (MM) aligned in a mostly north-south direction with an azimuthal angle of 204°. We determine and analyse the hourly mean ($\bar{A}$) and deviation (δ) of the signal amplitude in conjunction with solar-geomagnetic indices for the period around selected geomagnetic storms. Thereafter, we analysed the variations in electron density profiles and vertical TEC (VTEC) obtained from stations around the signal propagation paths.

2.2 Solar activity and associated geomagnetic variability

We also analyse solar-geomagnetic parameters around intervals of selected geomagnetic storms, to describe the prevailing space weather condition at the time. The utilised data include solar wind speed (V_{sw}) and particle density (PD), disturbance storm time (Dst), IMF B_y and B_z, and auroral electrojet (AE) index, from the the OMNI solar wind 1 AU data upstream, $https://omniweb.gsfc.nasa.gov/form/omni\_min.html$. Gonzalez et al. (1994) defined a geomagnetic storm as "an interval of time when a sufficiently intense and long-lasting interplanetary convection electric field leads, through a substantial energization in the magnetosphere-ionosphere system, to an intensified ring current strong enough to exceed some key threshold of the qualifying storm time Dst." Dst is a 1-hour index of magnetic activity derived from a network of near-equatorial geomagnetic observatories that measures the intensity of the assumed globally-symmetrical equatorial electrojet, or ring current (Rostoker, 1972). The Dst index is a negative deflection, in nT, of the horizontal magnetic field near the earths surface. Geomagnetic storms are classified according to Dst wherein a magnetic storm with a Dst between -30 and -50 nT is considered minor whereas a storm with a Dst from -50 to -100 nT is moderate and below -100 nT in intense. Addition classifications (Loewe & Prölss, 1997) rate the rare occurrence of larger geomagnetic storms as severe (DsT < -200 nT) and as great (Dst < -350 nT). AE index is most often associated with substorms and the dynamics of the magnetotail (Lakhina et al., 2006). Coupling between disturbances in the solar wind and the terrestrial magnetosphere are increased when the B_z component is negative. The B_y component affects the morphology of plasma flows at high latitudes and, while provided for the sake of completeness, the IMF B_y is of little consequence in the present study.

In the present work we examine the dayside (and dusk-to-dawn) responses of the D-region to four geomagnetic storms on 17, 26 September, 25 October and 1 November 2011 as the Sun was trending towards the solar maximum of cycle 24. Two of the storms were classified as moderate (-50 < Dst < -100 nT) with the remaining 2 classified as intense (Dst < -100). Details are provided in Table 2. In addition to the minimum Dst we list the maximum 3-hour a_p and related K_p indices (Rostoker, 1972) experienced at the height of the storm along with the state of the magnetosphere in accordance with the derivative NOAA Space Weather Scales. Of the 4 geomagnetic storms only the storm that peaked on 26 Oct 2011 would be classified as strong (G3) and expected to have a significant impact of modern technology systems (Odenwald, 2015). We note that the indices (V$_s w$, PD, Dst, B$_y$, B$_z$, and AE) used here are the 1-hour averaged. Therefore, variation in parameters are associated with the approximated time (in hour) against which they are recorded (in UT).

3 Analysis of prevailing space weather conditions

3.1 Geomagnetic storms of 17 September 2011

Figure 2 shows 1-hour averaged variations in solar wind speed (V_{sw}), particle density (PD), disturbance storm time (Dst), IMF B_y and B_z, and AE indices during 16 to 19 September 2011. A geomagnetic storm occurred on 17 September 2011. The minimum and maximum Dst values were -50 nT and -72 nT, respectively. The peak of the storm occured around 3:00 pm lasting for about 8 hours. The storm was preceded by a simultaneous increase in V_{sw} and PD from about 367 kms^{-1} and 3.6 Ncm^{-3} at around 3:00 am to respective peaks of 544 kms^{-1} (at around 12:00 noon) and 12.5 Ncm^{-3} at around 2:00 pm. This storm was caused by CME-driven interplanetary shocks (IPS), and reckoned among storms that marked the commencement of solar activity in the 24 solar cycle (Wu et al., 2016). Two CMEs of about 400 kms^{-1} (each) were recorded around 1:54 am and 9:54 pm on 14 Sept. 2011, which arrived Earth on 17 September and resulted in IPS that triggered this storm. The southward turning of the IMF B_z at around 7-8 am and consecutive fluctuations resulted in corresponding sudden commencemmnt of the storm with saw-toothed hourly variations in Dst (associated with the B_z fluctuations). The scenario suggests an intermittent magnetic reconnection and consequent energy tranfer from the solar wind to magnetosphere-ionosphere system. The auroral electrojet (AE) also significantly fluctuated between 3:00 am and 10:00 pm (due to the geomagnetic disturbance), increasing from 66 nT to 1063 nT. This indicates a strong coupling between the interplanetary magnetic field and the earth's magnetosphere-ionosphere system, and enhanced Ionospheric currents (in the auroral zone).

3.2 Geomagnetic storms of 26-27 September 2011

The geomagnetic storm of 26-27 September 2011 was relatively large storm with maximum Dst of -118 nT, which commenced at around 4:00 pm on 26 September and reached the peak around 11:00 pm. In Figure 3 we show the 1-hour averaged variations in V_{sw}, PD, Dst, B_y and B_z, and AE indices during 25 to 28 September 2011. The initiation of the storm appear to be similar to that of 17 September 2011. It was preceded by a simultaneous increase in V_{sw} and PD from 333 kms^{-1} and 12.9 Ncm^{-3} at around 11:00 am. V_{sw} reached a double peak of 686 and 688 kms^{-1} at around 11:00 pm (26 Sept.) and 1:00 am (27 Sept.), respectively, then gradually decreased until late 28 September, while PD significantly fluctuated after reaching two sharp peaks of 27.0 Ncm^{-3} and 24.4 Ncm^{-3} at around 1:00 pm and 3:00 pm, respectively. Similar to 17 September storm, this storm was caused by the arrival (on 26 Sept) of two CMEs, which occurred on 24 September at around 12:54 pm and 7:00 pm with speed of about 1050 kms^{-1} and 1065 kms^{-1}, respectively (see, table 1 in Wu et al. (2016)). The IPS driven by the CMEs arrived Earth at ∼12:40 pm leading to this sudden storm commencement (Wu et al., 2016; Correia et al., 2017). The storm commenced when the IMF B_z turned southward around 2-3:00 pm and reached the hourly averaged value of 12 nT at around 4:00 pm, and then turned northward at around 5:00 pm. The B_z turned southward again after 6:00 pm and reached second minimum value of $\sim$ 24.4 nT (averaged). When the B_z turned northward again at around 7:00 pm and relatively stabilised the storm entered a recovery phase until 1:00 pm on 27 September. A recurrent storm was also observed on 28 September probably triggered by significant increase in mean PD of up to 17.6 Ncm^{-3} (notwithstanding the gradual decrease in V_{sw}). Auroral activity (via AE) increase due to the storm reaching a peak of 1842 nT at around 7:00 pm on 26 September with and significantly fluctuated thereafter until late 28 September, in correlation with PD variability.

Correia et al. (2017) used multi-instrument observations (e.g., ionosonde, riometer, and GNSS receivers) to study the responses of the ionosphere to the 26-27 September 2011 geomagnetic storms in middle and high latitudes in the Antarctica American and Australian sectors. As expected, their result showed that the ionosphere was dynamic, highly disturbed and structured as a result of solar wind coupling with the magnetosphere-ionospheric system during the storm. They observed and charaterised a combination of effects associated with storm-driven prompt penetration electric fields (PPEFs) and disturbance dynamo processes, including storm-density enhancements (SEDs) at middle latitudes in the dayside sector just after the onset of the main phase storm, and tongues of ionization (TOIs) as a function of storm time and location. PPEF is the prompt penetration electric field caused by the impact of solar wind (-Vsw∗Bz) that is the predominant process affecting the low latitude ionosphere during the first 2 or 3 hours of the main phase geomagnetic storm, after these hours the perturbations at low latitudes are due the effects of the DDEF (disturbance dynamo electric field), which generates TIDs at auroral region that propagates to lower latitudes. So the ionospheric perturbations at low and mid latitudes are a competition between these two processes that have different roles. PPEF in the daytime side is eastward and elevates the equatorial ionosphere intensifying the fountain effect while in nighttime side is westward and pulls the ionosphere down. The DDEF operates exactly in the contrary way, pulls the ionosphere down during daytime and up in the night side.

3.3 Geomagnetic storms of 24-25 October 2011

The geomagnetic storms of 24-25 October 2011 (in the severe category) is the largest of the four storms considered in this work. Figure 4 shows 1-hour averaged variations in V_{sw}, PD, Dst, B_y and B_z, and AE indices during 24 to 27 October 2011. The storm commenced when B_z turned southward at around 11:00 pm (24 Oct.) and reached its peak (minimum Dst) around 1:00 am (25 Oct.) with mean Dst of -147 nT. A simultaneous and abrupt increase in V_{sw} and PD preceded the storm; V_{sw} increased from 377 kms^{-1} around 6:00 pm on 24 Oct. to over 500 kms^{-1} until 2:00 pm on 25 Oct. when the parameter fluctuated and then increased again to a mean peak of 534 kms^{-1} around 6:00 pm, while PD increase from 14 Ncm^{-3} at around 6:00 pm to maximum value of 27.9 Ncm^{-3} around 10:00 pm on 24 Oct. This storm was caused by the arrival of IPS (on 24 Oct.) driven by a Halo CME with speed exceeding 1000 kms^{-1} in association with M1.3 long duration solar flare at about 10:24 am on 22 Oct. (Blanch et al., 2013; Center, 2007). The B_z turned southward at around 22:00 pm (reaching the averaged minimum of -13 nT at 11:00 pm) in response to the solar wind condition, leading to the storm commencement. The B_z turned northward after 12:00 midnight on 25 Oct. and continue to increase, reaching a maximum of 21.3 nT at 12:00 noon. This scenario resulted to accelerated recovery during 6:00 am - 12:00 noon (25 Oct.). Therefter, the storm phase slowly recovered until 7:00 am on 27 Oct when the Dst increased to > -50 nT. The AE abruptly increased from 157 nT to 847 nT at around 6:00 pm (almost in synchrony with Vsw and PD), reaching a peak of 1042 nT at 12:00 midnight (25 Oct.). Although the AE fluctuated bewtween 7:00 pm (24 Oct.) and 8:00 am (25 Oct.), the value remained elevated during the interval. Blanch et al. (2013) investigated the effects of this storm on the ionosphere and the geomagnetic field using model and ground ionosonde data from both southern and northern hemispheres at Ebre Observatory and Port Stanley locations. They showed that variation in the ionospheric parameters reflected the geospheric effects of this geomagnetic storm. In particular, f_0F2 and h_mF2 increased at Ebre and Port Stanley, unmasking a positive storm effect which was attributed to traveling atmospheric disturbances (TADs) that are excited by energy injection from high latitudes. They also observed negative storm effect at Port Stanley associated with atmospheric composition changes that are related to the global thermospheric circulation.

3.4 Geomagnetic storms of 01-02 November 2011

Figure 5 shows 1-hour averaged variations in V_{sw}, PD, Dst, B_y and B_z, and AE indices during 29 October to 2 November 2011. The geomagnetic storm of 01-02 November 2011 was relatively a mild storm (the smallest of the cases considered) having minimum Dst value of -66 nT at 3:00 pm on 1 November. Although values of the parameters were relatively low, it is interesting to see that the interval was marked with significant fluctuation in geophysical parameters. It appears that energy began building up in the magnetosphere-ionosphere system after the first significant spike in V_{sw} and PD around 10:00 am on 30 Oct. until around 10:00 am on 1 Nov. when the storm was triggered following sudden increased in V_{sw} and southward turning of the B_z. A recurrent storm was also observed on 2 November. The AE increased to a peak of 978 nT and remained elevated throughout the storm phase on 1 Nov. but also significant fluctuated between 10:00 am on 30 Oct. (following the spike in V_{sw} and PD) and 7:00 pm on 2 Nov. (after the recurrent storm recovery).

4 Results and Discussion

4.1 Analysis of VLF amplitude variations associated with the geomagnetic storms

4.1.1 Variations in VLF amplitude during 17 September 2011 storm

Figure 6 shows the variation in Dst, AE, B_y and B_z, and 1-hour averaged values of VLF amplitude for DHO-A118, GQD-A118, NAA-A118 and NAA-ROI propagation paths during 16-19 September 2011. Each blue bar represent 1-hour mean amplitude, while the red dotted bar represent corresponding deviation (σ) or fluctuation. Our goal is to monitor the trend in amplitude variation during the storms interval. We analyse four days data in each case (with exception of 1 Nov. storm), starting 1-2 days before the storm (except for 25 Oct. storm) and 1-2 days after the storm. We observe small but obvious reduction in the daytime amplitude on the storm day (17 Sept.) in DHO-A118, NAA-A118 and NAA-ROI propagation paths (see, fig 6). Although the storm day amplitude for the GQD-A118 propagation path appear to be at the same level with the pre-storm day amplitude, further analysis (soon to follow) showed a minute decrease in the signal. The dusk-to-dawn (DTD) VLF signal amplitude is usually marked by large and rapid swings (or fluctuation) in signal strength (V. U. Nwankwo et al., 2016). In the night-side the reflection of the signal occurs from the lower part of the E-layer at around 90 km to 100 km altitude, since the D-layer (mainly ionised by Solar Ultra Violet rays) usually disappears after sunset (Abbey et al., 2015). Clearly, fluctuation in DTD signal is larger in NAA-A118 propagation path (as shown by the high values in σ), followed by the DHO-A118.

In order to obtain a better view of how the signal varied in response to the changes induced on the ionosphere by the geomagnetic storm we noted values of 1-hour mean signal amplitude before sunrise (MBSR), the daytime signal mean amplitude (DTMA) and the mean signal amplitude after sunset (MASS) for the day before the storm and monitored the corresponding signal values during and after the storm. In figure 7 we show the variation in MBSR, DTMA and MASS for DHO-A118, GQD-A118, NAA-A118 and NAA-ROI propagation paths during 16-19 September 2011. The two important days are 16 September (day before the storm) and 17 September (storm day). The storm days value are indicated by the red bar. We observed a reduction in MBSR in DHO-A118 and NAA-A118 propagation paths on the storm day by 4.34 dB and 2.39 dB, respectively. The signal MBSR remained at the same level with pre-storm day signal (16 Spetember) in the GQD-A118 propagation path but increase on the storm day in NAA-ROI path by 4.32 dB. The DTMA decreased in all the propagation paths (DHO-A118, GQD-A118, NAA-A118 and NAA-ROI) on the storm day by 3.04 dB, 0.21 dB, 2.01 dB and 2.10 dB, respectively. The MASS also decreased on the storm day in DHO-A118, GQD-A118 and NAA-ROI on the storm day by 2.05 dB, 2.09 dB and 2.29 dB, respectively, but increased in the NAA-A118 propagation path signal by 1.68 dB. This portion of result (with figure 6) was featured in SCOSTEP/PRESTO Newsletter (Vol. 23, p.10) as "Highlight on Young Scientists" because we started the work at the Centro de Rádio Astronomia e Astrofísica Mackenzie (CRAAM) São Paulo, SP, Brazil under the SCOSTEP Visiting Scholar (SVS) Programme.

4.1.2 VLF amplitude variations during 26-27 September 2011 storm

Figure 8 shows the variation in Dst, AE, B_y and B_z, and 1-hour averaged values of VLF amplitude for DHO-A118, GQD-A118, NAA-A118 and NAA-ROI propagation paths during 25-28 September 2011. Our result show a large decrease in DHO-A118 signal on the storm day (26 September) and a small decrease in GQD-A118. This significant 'dip' in DHO-A118 was also reported in Nwankwo et al. (2016). The data gap between 1:00 pm and 8:00 pm on 26 September in NAA-A118 and NAA-ROI propagation paths makes it difficult to compare their storm day signal level with those of pre-storm day. However, we compare values of the 12th- (12:00 noon) and 21st-hour (9:00 pm) mean amplitude on 25 Sept. (pre-storm) with those of 26 Sept. (storm day), and treated them as the DTMA and MASS, respectively, in the analysis to follow. We also observe a relatively larger fluctuation (marked by red dotted bar) in almost all the propagation paths during this interval (when compared with the smaller storm case during 16-19 Sept interval). The fluctuations may be related to the magnitude of the disturbances produced by this larger storm on the magnetosphere-ionosphere system, and coupled to the lower ionospheric region. The ionosphere was dynamic, highly driven (or disturbed) and structured during the 27 September 2011 storm (Correia et al., 2017).

In Figure 9 we show the variation in MBSR, DTMA and MASS for DHO-A118, GQD-A118, NAA-A118 and NAA-ROI propagation paths during 25-28 September 2011. There is a reduction in MBRS signal level in three of the four propagation paths on the storm day; the signal reduced by 0.48 dB, 1.41 dB and 11.86 dB in DHO-A118, GQD-A118 and NAA-ROI propagation paths, respectively, while the NAA-A118 increased by 3.62 dB. The DTMA decreased in all the propagation paths on the storm day by 15.96 dB, 0.8 dB, 1.74 dB and 1.48 dB, respectively. Variations in DTMA in NAA-A118 and NAA-ROI propagation paths are based on 12:00 noon values. The MASS value decreased in DHO-A118 and NAA-ROI by 16.17 dB and 16.07 dB, respectively, but increased in the GQD-A118 and NAA-A118 paths by respective values of 1.08 dB and 4.61 dB.

4.1.3 VLF amplitude variations during 24-25 October 2011 storm

Figure 10 shows the variation in Dst, AE, B_y and B_z, and 1-hour averaged values of VLF amplitude for DHO-A118, GQD-A118, NAA-A118 and NAA-ROI propagation paths during 24-27 October 2011. The storm, which commenced around 11:00 pm on 24 October (lasted for several hours into 25 October) is in the severe storm category and the largest of the four storms considered in this work. During this interval there were problems with the VLF signals received at ROI and A118 stations (from GQD and NAA transmitters), while DHO-A118 path has data covering the analysed interval. It is not clear whether the data gap in 3 of the 4 propagation paths is related to space weather-induced effects. This categary of storms (G3) are known to significantly impact modern technology systems (Odenwald, 2015). Although Blanch et al. (2013) reported absorption of radio waves in the lower ionosphere around the period due to solar flare-enhanced ionization from the X-ray solar burst, investigation into the possible cause of such anomaly is beyond the scope of this paper. For this storm, there is a large decrease in the signal level of DHO-A118 path, as well as significant signal fluctuations. The diurnal signal amplitude dropped to negative values on the storm day, and appear to gradually rise (or recover) in post-storm days (26-27 Oct.). This behaviour was perceive as the signal's tendency to recover to pre-storm day level (V. U. Nwankwo et al., 2016). Although the data inadequacy in GQD-A118, NAA-A118 and NAA-ROI paths makes it difficult to analyse their MBSR, DTMA and the MASS, analysis showed decrease in MBSR, DTMA and the MASS by 2.62 dB, 11.53 dB and 4.57 dB, respectively in DHO-A118 propagation path on the storm day.

4.1.4 VLF amplitude variations during 01-02 November 2011 storm

Figure 11 shows the variation in Dst, AE, B_y and B_z, and 1-hour averaged values of VLF amplitude for DHO-A118, GQD-A118, NAA-A118 and NAA-ROI propagation paths during 29 October - 02 November 2011. Although the geomagnetic storm (on 1 Nov.) associated with this interval is the smallest of the four cases analysed in this work, the geophysical features are of interest. There was a signicant fluctuation in solar-geomagnetic parameters during the 2 days preceding the storm and after the storm, due to the condition of the solar wind (also see, figure 5). We have added relatively undisturbed day (29 Oct.) to this disturbed interval in order to obtain and compare the quiet day signal levels with those of the storm day. Following a spike in the geophysical parameters (Dst, AE, By and Bz) on 30 Oct. we observed unusual fluctuation in the hourly mean signal in all the propagation paths with some dropping to negative values before the sunset teminator (e.g., DHO-A118, GQD-A118 and NAA-A118); the 16th, 17th and 21st bar are the respective reference sunset taminators (SST) for DHO-A118, GQD-A118 and NAA-A118. As the disturbance progressed into 31 Oct. the daytime signal level dropped to negative values in DHO-A118 propagation path, and significantly fluctuated in GQD-A118 path. The signals (in both paths) also fluctuated on the storm day (1 Nov.) but with lesser magnitude. In the analysis to follow (on MBSR, DTMA and MASS), we exclude 31 Oct. because the data obtained on the day between 8:00 am and 9:00 pm for NAA-A118 and NAA-ROI propagation paths are inadequate.

Figure 12 show variations in MBSR, DTMA and MASS for DHO-A118, GQD-A118, NAA-A118 and NAA-ROI propagation paths during 29 October - 02 November 2011 (excluding 31 October). When compared with pre-storm (and relatively quiet) day level, the results show reduction of the MBSR in DHO-A118, GQD-A118, NAA-A118 and NAA-ROI propagation paths by 11.86 dB, 2.25 dB, 4.3 dB and 28.28 dB, respectively. The DTMA signal dropped by 1.33 dB, 4.22 dB and 5.03 dB in DHO-A118, NAA-A118 and NAA-ROI, respectively, but increased slightly in GQD-A118 path by only about 0.19 dB. Reduction in MASS occurred in DHO-A118, GQD-A118 and NAA-ROI paths by 2.47, 4.32 dB and 9.86 dB, respectively, while the level increased by 3.41 dB in NAA-A118 paths, respectively. This analysis is based on the comparison between the signal levels of the relatively quiet day (29 October) with those of the storm day (1 November), because the two days preceding the storm were signicantly disturbed. Also, the previous analysis (using figure 11) showed significant fluctuations in the mean signal amplitude on the days. The goal of this present analysis is to investigate the couple effect of this extended period of (30-31 Oct.) of geomagnetic disturbances preceding the storm on 1 November. As mentioned earlier, there appear to be a gradual energy build-up in the magnetosphere-ionosphere system from the moment of first spike in V_{sw} and PD around 10:00 am on 30 Oct. until the storm was triggered on 1 Nov. following sudden increased in V_{sw} and southward turning of the B_z. From the foregoing analysis, the VLF signal fluctuations appear to reflect the pre-storm, storm- and post-storm day geomagnetic disturbances that are coupled to the ionosphere. The combined behaviour of the MBSR, DTMA and MASS in the four storm cases studied here are summarised in Table 3.

When the signal amplitude of pre-storm day (of relative quiet interval) were compared with the storm day values, most of the results presented here have shown decrease in the strength of the signal metrics. For the signal metrics analysed (from all propagation paths) the ratio of the storm day signal metric decrease (SDSD) to the total number of points (TNoPs) are 0.7692, 0.9231 and 0.6154 for MBSR, DTMA and MASS, respectively, while the respective ratio of storm day signal metric increase (SDSI) to the TNoPs are 0.1538, 0.0769 and 0.3846.

4.2 Analysis of Total Electron Content (TEC) dynamics during geomagnetic storms over the VLF propagation paths

In this section, we study the state of the ionosphere over the VLF propagation paths using the total election content (TEC) obtained from multiple GNSS/GPS stations near the transmitters and/or and receivers. Data from up to eleven (11) stations were analysed (8 in Europe, 2 the United States and 1 in Brazil). However, we select and present the results from only six (6) stations because the TEC profile of some stations are quite similar with those within short distances away. Details of the selected GNSS/GPS stations are provided in Table 4, and co-located on the maps in figure 13. We treat HERT, EUSK and ESCO stations as nearest to GQD-A118, DHO-A118 and NAA-A118 propagation paths, respectively, and OPMT station as being at the centre of the two transmitters (DHO and GQD) and receiver (A118) in the European sector. CHPI station is both near the ROI receiver and the NAA-ROI propagation path in Brazil (South America), while EPRT (and BARH) is near the NAA-A118 (and NAA-ROI) propagation path in the United States (North America). Figure 14 shows the contour plots of the interval of days analysed (to study storms), for the 6 TEC stations (HERT, EUSK, OPMT, ESCO, EPRT and CHPI). Although with varying intensity, the TEC variation in all the stations generally show both the local daytime increase and the additional enhancement (or increase) associated with the storms (day 2 in the European sector and day 3 in the American sector) on 17 and 26 September, 25 October and 1 November 2011. The daytime contour features observed almost in all stations (e.g., dumb or double-actagonal well shape on 17 and 25-26 September) appear to reflect the prevailing geomagnetic variability via the signature of Dst and B_y indices (see, figures 2-5).

In the European sector, Euskirchen region (EUSK station in Germany) near the DHO-A118 propagation path show largest storm-time increase or enhancement in the daytime TEC (see, figure 14(b)), followed by the Naut Aran axis (ESCO station in Spain) near the A118 receiver in Muret, France (figure 14d). It is difficult to ascertain the TEC profile at the central axis (OPMT station in Paris) during 24-27 October due to data gap, but 17-19 and 25-28 September intervals show very small difference between the TEC profile of Paris and that of Haisham axis (HERT station in London, UK) near the GQD-A118 propagation path. Figure 14e and 14f show the TEC profile of Eastport in Maine (USA) and Cachoeira Paulista in Sao Paulo (Brazil), 32.2 km and 166.66 km from the transmitter and receiver, respectively. Data show a reduced TEC responses during the strong storms on 26 September and 25 October near the NAA transmitter in the North American region (when compared to the scenarios in the European sector), while the scenario near the ROI receiver (in South American Brazilian region) show a very strong enhancement in TEC that are relatively larger than those of the European sector. Surprisingly, the TEC responses during the relatively small storm on 17 September in both North and South American sector appear to surpass those of the European sector (and its local 26 September and 25 October responses). The electron density profile during 31 October - 3 Novenber were comparatively low in all cases/regions (except Cachoeira Paulista in Brazil). Comparing the state of the ionosphere around the three transmitters (DHO, GQD and NAA) and two receivers (A118 and ROI), we suggest that transmitted signals appear to be significantly influenced by conditions in both 'local ionsphere' around the transmitter and along the propagation path until received at the receiver.

4.3 VLF amplitude anomalies in NAA-ROI propagation path associated with the storms

To further justify the observed decrease in VLF signal strength following a storm, we compare the diurnal amplitude variations of the four propagation paths (Figure 15). We present one more finding made in the course of this work. By plotting and comparing the diurnal amplitude variations of the four propagation paths (as shown in figure 15) we observe large fluctuation in NAA-ROI path signal during the 17 September and 25 October 2011 geomagnetic storms. Fluctuation of lesser magnitude also occurred during the storm of 1 November 2011. Because the data for the NAA-ROI during 26 September storm are inadequate, the diurnal amplitude for day is not included. We also compared the pre-storm and post-storm diurnal signals with these storm-day scenarios (data not included here) and found that the distinction remained. Although this observed anomaly is distinctively larger, Peter et al. (2006) also reported similar fluctuations (of lesser magnitude), during geomagnetic storms of 7 April 2000 and 31 October 2003.

In order to ascertain the veracity of associating this observation with the storms, it is however, important to investigate the possible influence of other phenomena (such as Gravity Waves) on the signal during these intervals. Gravity Waves can influence the conditions of the electron density at reflection height of the VLF signals, and consequently produce fluctuations of the electrical conductivity that can also be detected as variations in the VLF amplitude and phase (Correia et al., 2020). Such investigation is beyond the scope of this work. However, data showed strong enhancement of electron density profiles near the ROI receiver (that are relatively larger than those of the North American (Maine) and European sector), suggesting that the ionosphere was markedly different along the ROI receiver.

4.4 Large amplitude variation in DHO-A118 propagation path associated with the storms

Figure 16 provides an overview of the VLF amplitude data acquired on the DHO-A118 link for the four intervals listed in Table 2. The Dst index was previously discussed in general. Each of the Dst plots shows the progression of the storms in term of its onset (initial increase in Dst), main phase (negative bay), and recovery (return to a normal baseline). For each of the storms the associated Sudden Storm Commencement (SSC) is indicated above the panel. Also indicated below each of the data plots are indications if and when a solar particle event (SPE) was in process. In Table 5 we show the ancillary information related to the timing, classification and location of associated solar flares, CMEs if and when first observed lifting off the sun, solar particle events (SPEs) if detected, and the timings for the SSCs. The ancillary data were obtained from a variety of the authoritative sources as noted in the Acknowledgement section. Clearly the remarkable reduction in the dayside signal of the DHO-A118 propagation path can be seen in figure 16. Strong storms show even larger reduction (also see, figures 8 and 10). The signal strength decreased by about 3.04 dB, 15.96 dB, 11.53 dB and 1.33 dB on 17, 26 September, 25 October and 1 November storms, respectively.

Interestingly, the regions near the DHO-A118 path (Euskirchen) have also shown strong enahancement in daytime TEC than the three other regions in European sector during the two storms. It is worth to mention that the TEC data obtained from other stations around the DHO-A118 propagation paths (shown in Figure 17) show similar profile as that of EUSK (e.g., REDU (Redu), DOUR (Dourbes), TITZ (Titz) and SASS (Sassnitz Island of Ruegen), all in Germany). On this premise, we infer that this response of DHO-A118 path signal may be related to the larger enhancement of TEC (stonger ionospheric responses) near the DHO transmitter. It can also be seen from Table 5 and figure 16 that the large increase (15.96 dB and 11.53 dB) that occurred in DHO-A118 propagation paths on 26 September and 25 October storms are associated with SPEs. This observation is in agreement with the work of Peter et al. (2006), who observed increases in the energetic electron flux (measured by the NOAA-POES satellites) and VLF signal depressions (and fluctuations) in mid-latitude associated with the geomagnetic storms on 7 April 2000 and 31 October 2003 (using VLF data from the Holographic Array for Ionospheric/Lightning Research (HAIL), located in the United States).

We now summarise our results by combining simultaneously observed dayside (8:00 am - 6:00 pm) signal amplitude in DHO-A118 with VTEC variations over the signal propagation paths. Unlike other propagation paths the DHO-A118 data is both availability and of good quality during all the storm intervals analysed in this work. Figure 18 show the plot of the daytime variation in VLF amplitude (red line plot) for DHO-A118 propagation path, together with VTEC values obtained from HERT (black line), EUSK (blue line), OPMT (green line) and ESCO (brown line) stations across Europe during 16-19 and 25-28 September, 24-27 October and 29 October-1 November 2011. There is general increase or elevation of VTEC values on storm days as can be observed in the figure. The 25 October geomagnetic storm actually commenced around 11:00 pm on 24 October (and reached its peak (or minimum Dst) around 1:00 am on 25 October), hence the depression observed in VTEC values of HERT, EUSK and OPMT stations. We note the dipping (or depression) of the daytime VLF amplitude on the storm days (as VTEC values increased accordingly). It can also be observed that the post-storm day signal tend to return (or recover) to the pre-storm day level. Although the scenario on 29 October - 1 November appear otherwise, the variations reflect the unique features of the interval (previously described in sections 3.4 and 4.1.4); because the two days preceding the storm were signicantly disturbed (analysis is based on the comparison between the signal levels of the relatively quiet day (29 Nov) with those of the storm day (1 Nov.)).

5 Conclusion

VLF radio waves are sensitive to the changes in electrical conductivity of the lower ionosphere, and therefore affected when propagating through the ionosphere (Alfonsi et al., 2008). As the conductivity of the ionosphere can also be influenced by different phenomena (e.g., solar flares, geomagnetic storms, lightening etc) the amplitude and/or phase of the waves can be monitored to identify possible anomaly or deviations from its diurnal signature in association with an event (driving ionospheric irregularities). However, since the use of single observational tool can be inadequate (due to the complex nature and temporal variability of the ionosphere), utilising a multi-tool approach that combines data from different ground-based and space-borne observation can be more effective for probing ionospheric irregularities. In this paper, we built on previous work to probe ionosphere responses to geomagnetic storms as it propagates down to the lower ionosphere from the magnetosphere, using data from VLF and GNSS/GPS receivers. We monitored the variations in diurnal amplitude of the VLF radio waves and analysed three metrics of the signals such as the MBSR, DTMA and MASS during intervals of 4 geomagnetic storms (on 17 and 26 September, 25 October and 1 November 2011). The signals of four propagation paths (i.e., DHO-A118, GQD-A118, NAA-A118 and NAA-ROI) were analysed for the intervals 16-19 and 25-28 September, 24-27 October and 29 October - 01 November, with respect to the storm days. When the VLF amplitude of the pre-storm day were compared with the storm day values, our results showed significant reduction in MBSR, DTMA and MASS signal strength in majority of the cases. The ratio of the SDSD to the TNoPs considered are 0.7692, 0.9231 and 0.6923 for MBSR, DTMA and MASS, respectively, while the respective ratio of storm day SDSI to the TNoPs are 0.1538, 0.0769 and 0.3846. Of the four propagation paths, the DHO-A118 path (in the European sector) showed the largest decrease especially during strong storms that are associated with SEP. We also observed distinct anormaly (large signal fluctuation) in NAA-ROI propagation path signal in South American Brazil region. We further investigated the state of the ionosphere over the VLF propagation paths using TEC data obtained from multiple GNSS/GPS stations near the transmitters and receivers, to understand these propagation characteristics. Data showed larger enhancement of electron density profiles near the DHO transmitter and ROI receiver, suggesting possible connection with strong storm responses leading to the large VLF amplitude decrease and fluctuation observed in DHO-A118 and NAA-ROI propagation paths. By combining simultaneously observed VLF amplitude variations in the D-region with VTEC data over the signal propagation paths, we presented strong and compelling evidence of storm-induced reduction of the amplitude of VLF signals, and confirms previous reports [e.g., (V. U. Nwankwo et al., 2016)]. However, it is worth to mention that some signal propagation paths may not exhibit this characteristics (storm-induced dipping), and/or may do so for some storms. Among others, factors such as mode interference, propagation path and anti-correlated responses of VLF signal to a combination of storm induced and/or enhanced ionospheric phenomena (e.g., PPEFs and DDEF), and strong solar flares occuring simultaneously can affect characteristic dipping. It is therefore important to closely monitor and/or investigate the state of the ionosphere over the propagation paths of VLF radio waves (as was done here) when using the data to probe ionospheric irregularities.

Acknowledgments

Victor U.J. Nwankwo acknowledge the Scientific Committee for Solar-Terrestrial Physics for the award of SCOSTEP Visiting Scholarship, during which this work was started at the host institute (Centro de Rádio Astronomia e Astrofísica Mackenzie, Universidade Presbiteriana Mackenzie, São Paulo, Brazil). Authors acknowledge the A118 SID VLF database (https://sidstation.loudet.org/data-en.xhtml), and VLF data from ROI station are available upon request by email to Emilia Correia (ecorreia@craam.mackenzie.br), NASA/GSFCs Space Physics Data Facilitys OMNIWeb service for the 1-hour averaged values of V_{sw}, PD, Dst, IMF B_y and B_z, and AE (*https://omniweb.gsfc.nasa.gov/form/omni_min.html*), and Scripps Orbit and Permanent Array Center (SOPAC) for TEC/VTEC data (*http://sopac.ucsd.edu/sopacDescription.shtml*). J.-P. Raulin acknowledges CNPq (contracts 312066/2016-3). The research leading to these results has received funding from CAPES grant 88881.310386/2018-01. Emilia Correia also thanks the National Council for Scientific and Technological Development - CNPq (processes no: 406690/2013-8 and 306818/2019-1) and So Paulo Research Foundation FAPESP (process no: 2019/05455-2) for individual research support.

References

Abbey, T., Cook, J., Farn, D., Jones, T., Kinder, M., Lutley, A., ... C, R. W. T. (2015). *Very low frequency receiver - user manual.* UK Radio Astronomy Association (UKRAA), Surrey, UK, *https : //www.ukraa.com/downloads/manuals*.

Abd Rashid, M. M., Ismail, M., Hasbie, A. M., Salut, M. M., & Abdullah, M. (2013). Vlf observation of d-region disturbances associated with solar flares at ukm selangor malaysia. In *2013 ieee international conference on space science and communication (iconspace)* (pp. 249–252).

Adeniyi, J., Doherty, P., Oladipo, O., & Bolaji, O. (2014). Magnetic storm effects on the variation of tec over ilorin an equatorial station. *Radio Science*, *49*(12), 1245–1253.

Alfonsi, L., Kavanagh, A. J., Amata, E., Cilliers, P., Correia, E., Freeman, M., ... others (2008). Probing the high latitude ionosphere from ground-based observations: The state of current knowledge and capabilities during ipy (2007–2009). *Journal of Atmospheric and Solar-Terrestrial Physics*, *70*(18), 2293–2308.

Anderson, T. S., McCarthy, M. P., & Holzworth, R. H. (2020). Detection of vlf attenuation in the earthionosphere waveguide caused by xclass solar flares using a global lightning location network. *Journal of Geophysical Research: Space Weather*, *18*(e2019SW002408).

Barr, R., Jones, D. L., & Rodger, C. (2000). Elf and vlf radio waves. *Journal of Atmospheric and Solar-Terrestrial Physics*, *62*(17-18), 1689–1718.

Berdermann, J., Kriegel, M., Banyś, D., Heymann, F., Hoque, M., Wilken, V., ... Jakowski, N. (2018). Ionospheric response to the x9. 3 flare on 6 september 2017 and its implication for navigation services over europe. *Space Weather*, *16*(10), 1604–1615.

Beynon, W., & Jones, E. (1965). Seasonal variations in the lower and upper atmosphere. *Nature*, *206*(4990), 1243–1245.

Blagoveshchensky, D. V., Maltseva, O. A., & Sergeeva, M. A. (2018). Impact of magnetic storms on the global tec distribution. In *Annales geophysicae* (Vol. 36, pp. 1057–1071).

Blanch, E., Marsal, S., Segarra, A., Torta, J., Altadill, D., & Curto, J. (2013). Space weather effects on earth's environment associated to the 24–25 october 2011 geomagnetic storm. *Space Weather*, *11*(4), 153–168.

Burešová, D., & Laštovička, J. (2007). Pre-storm enhancements of fof2 above europe. *Advances in Space Research*, *39*(8), 1298–1303.

Center, C. D. (2007). Soho lasco cme catalog. *URL: http://cdaw. gsfc. nasa. gov/CME_list/index. html*.

Chakrabarti, S. K., Acharyya, K., Bose, B., Mandal, S., Chatterjee, A., Nandi, N., ... Khan, R. (2005). Monitoring of sudden ionospheric disturbances (sid) from kolkata (india). *arXiv preprint astro-ph/0501289*.

Chapman, S. (1931). The absorption and dissociative or ionizing effect of monochromatic radiation in an atmosphere on a rotating earth. *Proceedings of the Physical Society*, *43*(1), 26.

Chisham, G., Lester, M., Milan, S., Freeman, M., Bristow, W., Grocott, A., ... others (2007). A decade of the super dual auroral radar network (superdarn): Scientific achievements, new techniques and future directions. *Surveys in geophysics*, *28*(1), 33–109.

Chuo, Y., Lee, C., Chen, W., & Reinisch, B. (2013). Comparison of the characteristics of ionospheric parameters obtained from formosat-3 and digisonde over ascension island. In *Annales geophysicae* (Vol. 31, pp. 787–794).

Correia, E., Raunheitte, L. T. M., Bageston, J. V., & D'Amico, D. E. (2020). Characterization of gravity waves in the lower ionosphere using very low frequency observations at comandante ferraz brazilian antarctic station. In *Annales geophysicae* (Vol. 38, pp. 385–394).

Correia, E., Spogli, L., Alfonsi, L., Cesaroni, C., Gulisano, A. M., Thomas, E. G., … Rodel, A. A. (2017). Ionospheric f-region response to the 26 september 2011 geomagnetic storm in the antarctica american and australian sectors. In *Annales geophysicae.*

Dahlgren, H., Sundberg, T., Collier, A. B., Koen, E., & Meyer, S. (2011). Solar flares detected by the new narrowband vlf receiver at sanae iv. *South African Journal of Science*, *107*(9-10), 40–47.

Ding, F., Wan, W., Liu, L., Afraimovich, E., Voeykov, S., & Perevalova, N. (2008). A statistical study of large-scale traveling ionospheric disturbances observed by gps tec during major magnetic storms over the years 2003–2005. *Journal of Geophysical Research: Space Physics*, *113*(A3).

Greenwald, R., Baker, K., Dudeney, J., Pinnock, M., Jones, T., Thomas, E., … others (1995). : Darn/superdarn a global view of the dynamics of high-latitude convection, space sci. rev., 71, 761-796.

Hargreaves, J., & Roberts, R. (1962). The propagation of very low frequency radio waves over distances up to 2000 km. *Journal of Atmospheric and Terrestrial Physics*, *24*(6), 435–450.

Hildebrand, V. (1993). Investigations of equatorial ionosphere nighttime mode conversion at vlf. *Had-A267 991*.

Ho, C., Mannucci, A., Lindqwister, U., Pi, X., Tsurutani, B., Sparks, L., … Reyes, M. (1998). Global ionospheric tec variations during january 10, 1997 storm. *Geophysical Research Letters*, *25*(14), 2589–2592.

Igarashi, K., Murayama, Y., Nagayama, M., & Kawana, S. (2000). D-region electron density measurements by mf radar in the middle and high latitudes. *Advances in Space Research*, *25*(1), 25–32.

Jain, A., Tiwari, S., Jain, S., & Gwal, A. (2010). Tec response during severe geomagnetic storms near the crest of equatorial ionization anomaly. *94.20. Vv; 94.30. Lr*.

Kikuch, T., & Evans, D. S. (1983). Quantitative study of substorm-associated vlf phase anomalies. *Journal of Geophysicsl Research*, *88*(A2), 871–4380.

Kleimenova, N., Kozyreva, O., Rozhnoy, A., & Solov'eva, M. (2004). Variations in the vlf signal parameters on the australia-kamchatka radio path during magnetic storms. *Geomagnetism and Aeronomy*, *44*(3), 354–361.

Komjathy, A., Sparks, L., Wilson, B. D., & Mannucci, A. J. (2005). Automated daily processing of more than 1000 ground-based gps receivers for studying intense ionospheric storms. *Radio Science*, *40*(06), 1–11.

Kumar, A., & Kumar, S. (2014). Space weather effects on the low latitude d-region ionosphere during solar minimum. *Earth, planets and space*, *66*(1), 76.

Lakhina, G., Alex, S., Mukherjee, S., & Vichare, G. (2006). On magnetic storms and substorms.

Laštovička, J. (1996). Effects of geomagnetic storms in the lower ionosphere, middle atmosphere and troposphere. *Journal of Atmospheric and Terrestrial Physics*, *58*(7), 831–843.

Loewe, C., & Prölss, G. (1997). Classification and mean behavior of magnetic storms. *Journal of Geophysical Research: Space Physics*, *102*(A7), 14209–14213.

Mannucci, A. J., Tsurutani, B. T., Kelley, M. C., Iijima, B. A., & Komjathy, A. (2009). Local time dependence of the prompt ionospheric response for the 7, 9, and 10 november 2004 superstorms. *Journal of Geophysical Research: Space Physics*, *114*(A10).

McRae, W. M., & Thomson, N. R. (2004). Solar flare induced ionospheric d-region enhancements from vlf phase and amplitude observations. *Journal of Atmospheric and Solar-Terrestrial Physics*, *66*(1), 77–87.

Mechtly, E., Bowhill, S., Smith, L., & Knoebel, H. (1967). Lower ionosphere electron concentration and collision frequency from rocket measurements of faraday rotation, differential absorption, and probe current. *Journal of Geophysical Research*, *72*(21), 5239–5245.

Mitra, A. P. (1974). Ionospheric effects of solar flares.

Nath, N., & Setty, C. (1976). The d-region ion composition. *pure and applied geophysics*, *114*(6), 891–908.

NGDC. (1994). *Ionospheric digital database - worldwide vertical incidence parameters.* National Oceanic and Atmospheric Administration (NOAA), Boulder, Colorado, USA.

Nicolet, M., & Aikin, A. (1960). The formation of the d region of the ionosphere. *Journal of Geophysical Research*, *65*(5), 1469–1483.

Nwankwo, V. U., Chakrabarti, S. K., & Ogunmodimu, O. (2016). Probing geomagnetic storm-driven magnetosphere–ionosphere dynamics in d-region via propagation characteristics of very low frequency radio signals. *Journal of Atmospheric and Solar-Terrestrial Physics*, *145*, 154–169.

Nwankwo, V. U. J. (2016). *Effects of space weather on earths ionosphere and nominal leo satellites aerodynamic drag* (Unpublished doctoral dissertation).

Nwankwo, V. U. J., Chakrabarti, S. K., Sasmal, S., Denig, W., Ajakaiye, M. P., Akinsola, T., ... others (2020). Radio aeronomy in nigeria: First results from very low frequency (vlf) radio waves receiving station at anchor university, lagos. In *2020 international conference in mathematics, computer engineering and computer science (icmceccs)* (pp. 1–7).

Odenwald, S. (2015). *Solar storms˜ 2000 years of human calamity! author: S. odenwald publisher: S. odenwald isbn: 978-1-505-941463 date publi.* S. Odenwald.

of the Federal Coordinator for Meteorological Services, O., & Research, S. (2013). Report on space weather observing systems: Current capabilities and requirements for the next decade.

Ohya, H., Shiokawa, K., & Miyoshi, Y. (2011). Long-term variations in tweek reflection height in the d and lower e regions of the ionosphere. *Journal of Geophysical Research: Space Physics*, *116*(A10).

Ouattara, F., Amory-Mazaudier, C., Fleury, R., Duchesne, P. L., Vila, P., & Petitdidier, M. (2009). West african equatorial ionospheric parameters climatology based on ouagadougou ionosonde station data from june 1966 to february 1998.

Pacini, A. A., & Raulin, J.-P. (2006). Solar x-ray flares and ionospheric sudden phase anomalies relationship: A solar cycle phase dependence. *Journal of Geophysical Research: Space Physics*, *111*(A9).

Peter, W. B., Chevalier, M., & Inan, U. S. (2006). Perturbations of midlatitude subionospheric vlf signals associated with lower ionospheric disturbances during major geomagnetic storms. *Journal of Geophysical Research: Space Physics*, *111*(A3).

Raulin, J.-P., Pacini, A. A., Kaufmann, P., Correia, E., & Martinez, M. A. G. (2006). On the detectability of solar x-ray flares using very low frequency sudden phase anomalies. *Journal of atmospheric and solar-terrestrial physics*, *68*(9), 1029–1035.

Rostoker, G. (1972). Geomagnetic indices. *Reviews of Geophysics*, *10*(4), 935–950.

Ruohoniemi, J., & Baker, K. (1998). Large-scale imaging of high-latitude convection with super dual auroral radar network hf radar observations. *Journal of Geophysical Research: Space Physics*, *103*(A9), 20797–20811.

Samanes, J., Raulin, J.-P., Cao, J., & Magalhaes, A. (2018). Nighttime lower ionosphere height estimation from the vlf modal interference distance. *Journal of Atmospheric and Solar-Terrestrial Physics*, *167*, 39–47.

Sica, R., & Schunk, R. (1990). Interpreting vertical plasma drift in the mid-lattitude ionosphere using ionosonde measurements. *Planetary and space science*, *38*(12), 1567–1571.

Tan, L., Thu, N., & Ha, T. (2014). Observation of the effects of solar flares on the nwc signal using the new vlf receiver at tay nguyen university. *Sun & Geosphere*, *8*(1), 27–31.

Thomson, N. R., & Clilverd, M. A. (2001). Solar flare induced ionospheric d-region enhancements from vlf amplitude observations. *Journal of Atmospheric and Solar-Terrestrial Physics*, *63*(16), 1729–1737.

Thomson, N. R., Clilverd, M. A., & Rodger, C. J. (2017). Midlatitude ionospheric d region: Height, sharpness, and solar zenith angle. *Journal of Geophysical Research: Space Physics*, *122*(8), 8933–8946.

Todoroki, Y., Maekawa, S., Yamauchi, T., Horie, T., & Hayakawa, M. (2007). Solar flare induced d region perturbation in the ionosphere, as revealed from a short-distance vlf propagation path. *Geophysical research letters*, *34*(3).

Verkhoglyadova, O., Tsurutani, B., Mannucci, A., Mlynczak, M., Hunt, L., Paxton, L., & Komjathy, A. (2016). Solar wind driving of ionosphere-thermosphere responses in three storms near st. patrick's day in 2012, 2013, and 2015. *Journal of Geophysical Research: Space Physics*, *121*(9), 8900–8923.

Wait, J. R. (1960). Terrestrial propagation of very-low-frequency radio waves, a theoretical investigation. *J. Res. Nat. Bureau Stand*, *64*, 153.

Wu, C.-C., Liou, K., Vourlidas, A., Plunkett, S., Dryer, M., Wu, S., ... Howard, R. A. (2016). Numerical simulation of multiple cme-driven shocks in the month of 2011 september. *Journal of Geophysical Research: Space Physics*, *121*(3), 1839–1856.

6 Tables

Table 1. Detail of transmitters, receivers and propagation paths of VLF data used in the study

Propagation path	Transmitter (T)			Receiver (R)			T-R Distance
Path	Acronym/Freq	Location	Coord.	Acronym	Location	Coord.	(km)
DHO-A118	DHO(23.4 kHz)	Rhauderfehn, Germany	53.0789°N, 007.6150°E	A118	Muret, France	43.4616°N, 1.3307°E	1169.18
GQD-A118	GQD(22.1 kHz)	Anthorn, Cumbria, UK	54.7317°N, 002.8830°W	A118	Muret, France	43.4616°N, 1.3307°E	1315.66
NAA-A118	NAA(24.0 kHz	Cutler, Maine, USA	44.6449°N, 067.2816°W	A118	Muret, France	43.4616°N, 1.3307°E	5308.42
NAA-ROI	NAA(24.0 kHz)	Cutler, Maine, USA	44.6576°N, 067.2039°W	ROI	Sao Paulo, Brazil	23.1175°S, 46.5560°W	7826.79

Table 2. Geomagnetic storm values for the intervals of interest.

Storm interval (2011)	Storm Maximum time	Minimum Dst (nT)	Maximum a_p (nT)
16-Sept to 19-Sept	17 Sep @ 24 UT	-72	56 (K_p = 5+/G1)
25-Sept to 28 Sept	26 Sep @ 17 UT	-118	94 (K_p = 6+/G2)
24-Oct to 27-Oct	26 Oct @ 02 UT	-147	154 (K_p = 7+/G3)
29-Oct to 02-Nov	01 Nov @ 01 UT	-66	39 (K_p = 5-/G1)

Table 3. Combined behaviour of the MBSR, DTMA and MASS metrics during the four geomagnetic storms. TNoPs=total number of points, SDSD=storm day signal decrease, SDSI=storm day signal increase

VLF Signal Metric	TNoPs	SDSD	SDSI	Unchanged	SDSD/TNoPs	SDSI/TNoPs
MBSR	13	10	2	1	0.7692	0.1538
DTMA	13	12	1	0	0.9231	0.0769
MASS	13	9	4	0	0.6923	0.3077

Table 4. Details of GNSS/TEC stations used and their approximate distances from transmitters (T), recievers (R) and propagation paths (T-R)

Station	Location	Coordinate	Nearest Transmitter (T)	Nearest Reciever (R)	Approx. dist. from T (km)	Approx. dist. from R (km)	Approx. dist. from Nearest PP (km)
EUSK	Euskirchen, Germany	50.657°N, 6.790°E	DHO	A118	279.99	900.78	77.08
HERT	Hailsham, UK	50.867°N, 0.334°E	GQD	A118	508.21	827.06	102.54
OPMT	Paris, France	48.836°N, 2.335°E	DHO/GQD	A118	598.65/774.96	605.34	156.01/212.30
ESCO	Naut Aran, Spain	42.693°N, 0.975°E	DHO	A118	1381.53	90.47	102.38
EPRT	Eastport, United States	44.909°S, -66.992°W	NAA	A118	32.20	5282.83	24.87
CHPI	Cachoeira Paulista, Brazil	-22.687°S, -44.986°W	NAA	ROI	7822.87	166.66	166.66

Table 5. Ancillary information of the timing, classification and location of associated solar flares, CMEs, SPEs, and the timings for the SSCs

Flare time	Flare Class	Group	Location	CME Time	CME Type	CME Speed	SEP	SSC
16/07 11:30	C9.3	11290	S12W59	xxxxx	xxxxx	xxxxx	no	17/09 03:43
22/09 10:29	X1.4	11302	N13E78	22/09 10:48	Halo	1905	23/09 22:55	26/09 12:34
24/09 09:21	X1.9	11302	N12E60	24/09 09:48	Partial Halo	1936	enhanced	xxxxx
22/10 10:00	M1.3	11314		22/10 10:24	Halo	1005	weak	24/10 18:31
31/10 17:21	M1.4	unknown	unknown	xxxxx	xxxxx	xxxxx	no	01/11 09:07

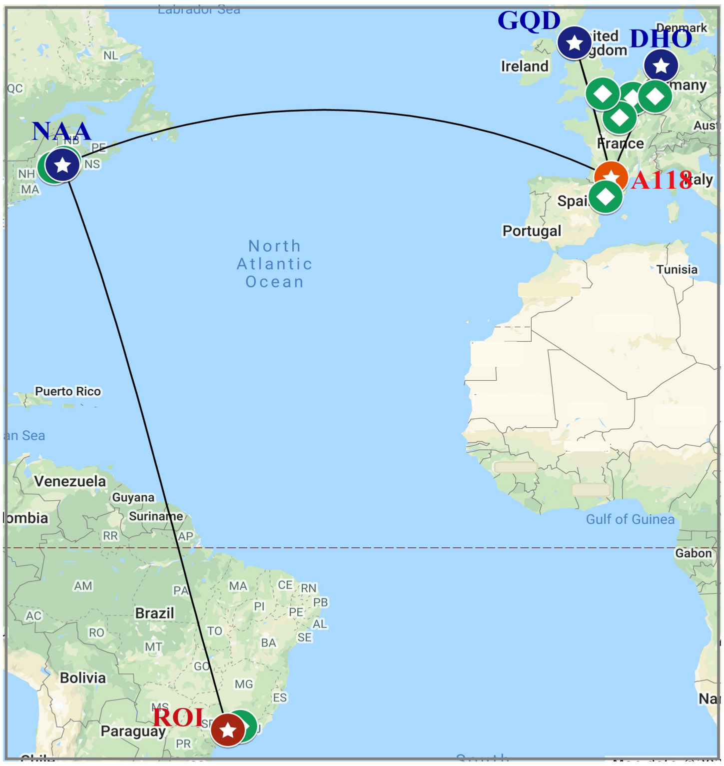

Figure 1. VLF signal transmitters (red stared circles), receiver (blue stared circles), propagation paths (black lines) and GNSS stations (green circles) used in the study.

842 # 7 Figures

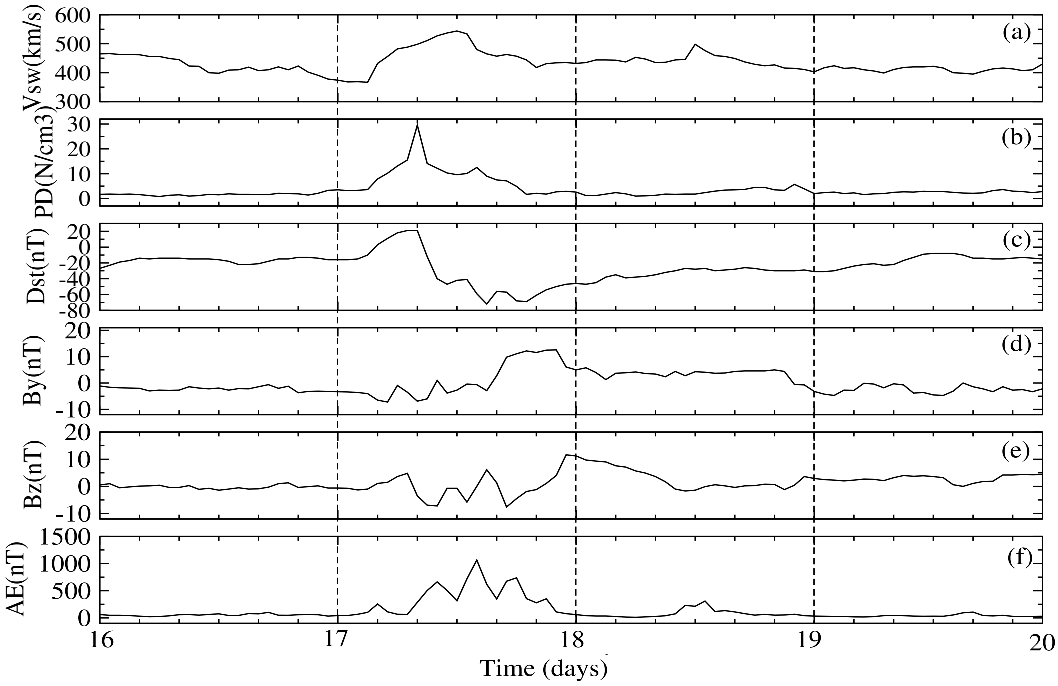

Figure 2. 1-hour averaged variations in solar wind speed (V_{sw}), particle density (PD), disturbance storm time (Dst), IMF B_y and B_z, and AE indices during 16 to 19 September 2011.

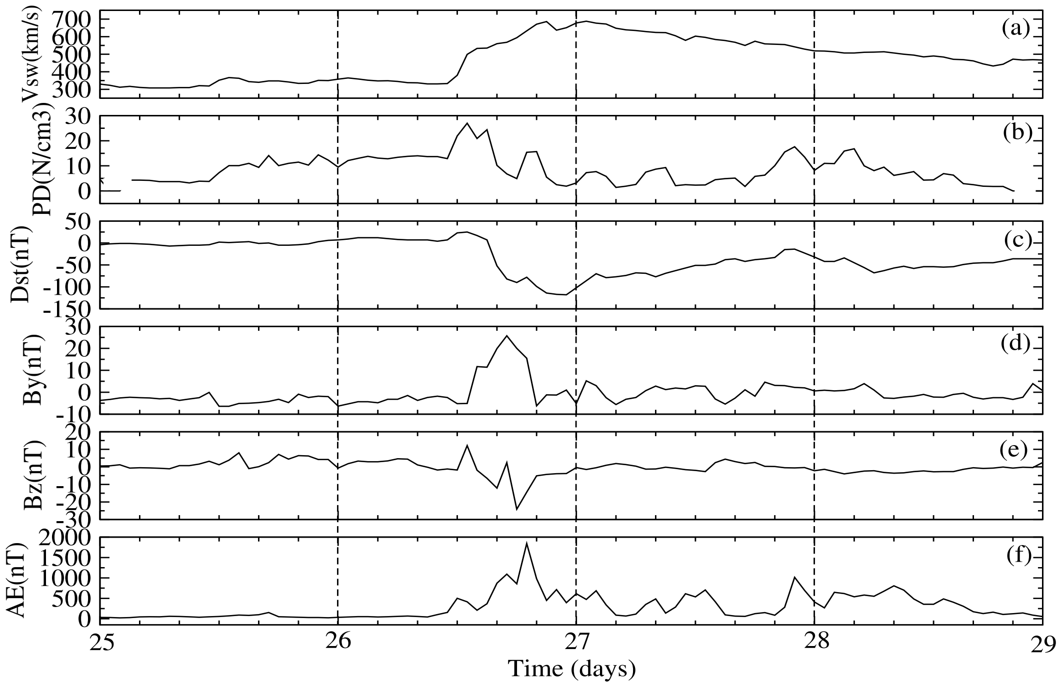

Figure 3. 1-hour averaged variations in V_{sw}, PD, Dst, B_y and B_z, and AE indices during 25 to 28 September 2011.

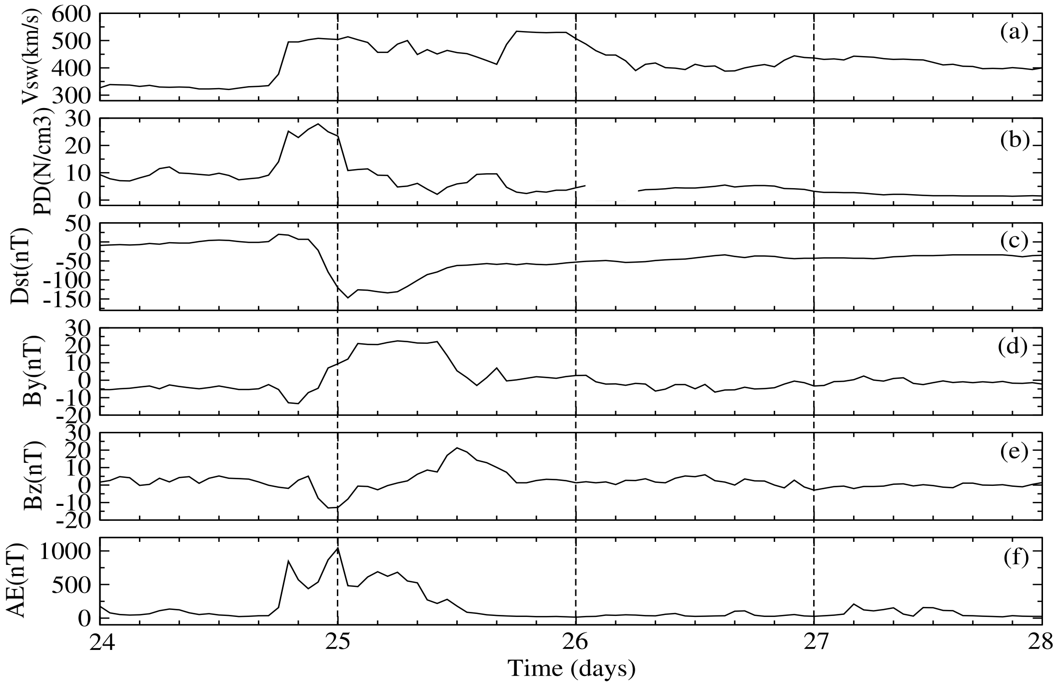

Figure 4. 1-hour averaged variations in V_{sw}, PD, Dst, B_y and B_z, and AE indices during 24 to 27 October 2011.

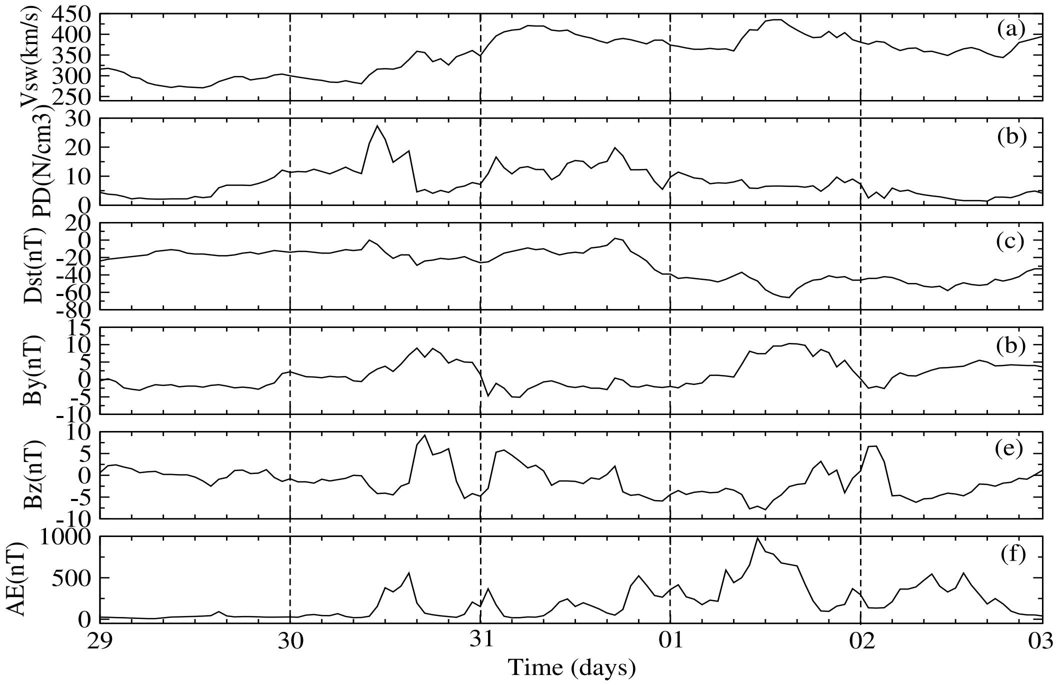

Figure 5. 1-hour averaged variations in V_{sw}, PD, Dst, B_y and B_z, and AE indices during 29 October to 2 November 2011.

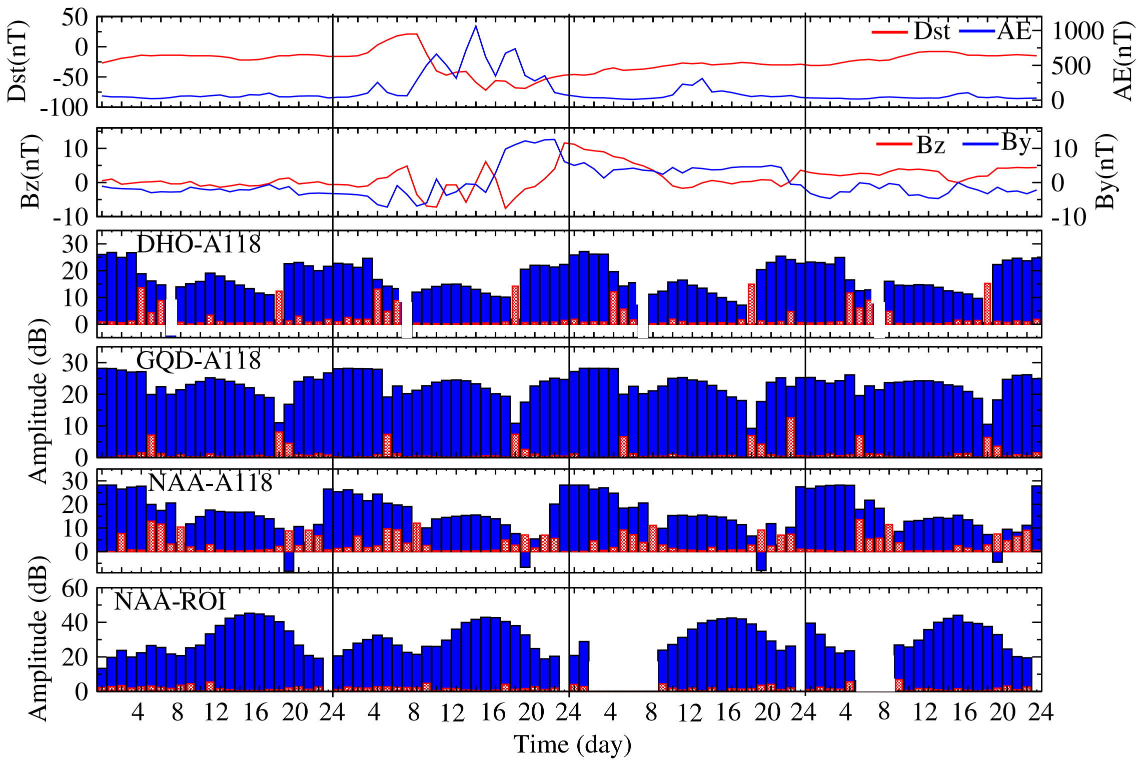

Figure 6. Variation in Dst, AE, B_y and B_z, and 1-hour averaged values VLF amplitude for DHO-A118, GQD-A118, NAA-A118 and NAA-ROI propagation paths during 16-19 September 2011. Each blue bar represent 1-hour mean amplitude, while the red bar represent the respective deviation (σ) or fluctuation.

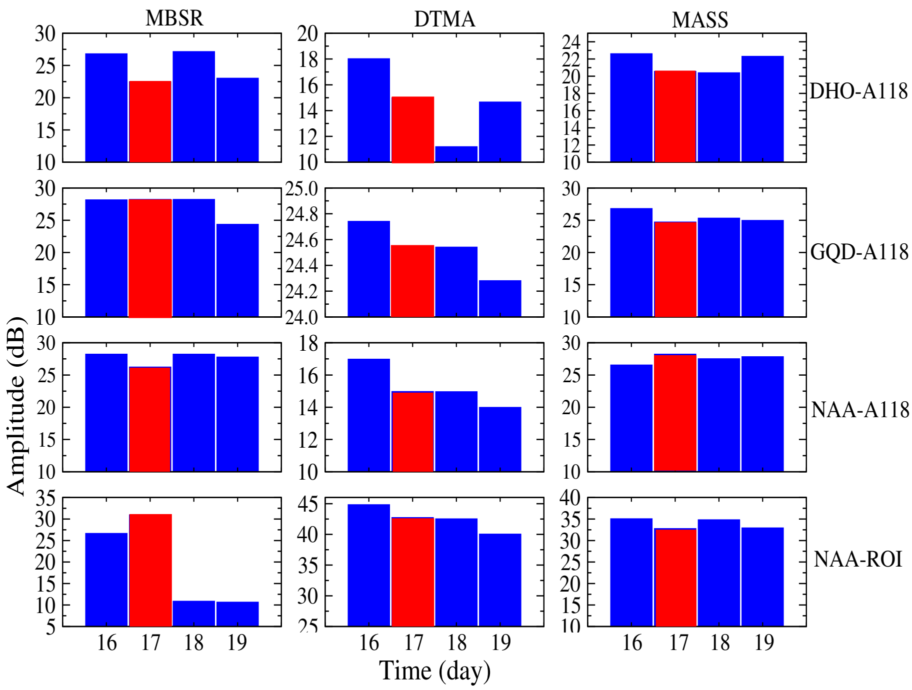

Figure 7. Variation in 1-hour mean signal amplitude before sunrise (MBSR), the daytime signal amplitude (DTMA) and the mean signal amplitude after sunset (MASS) for DHO-A118, GQD-A118, NAA-A118 and NAA-ROI propagation paths during 16-19 September 2011. The storm days value are indicated by the red bar

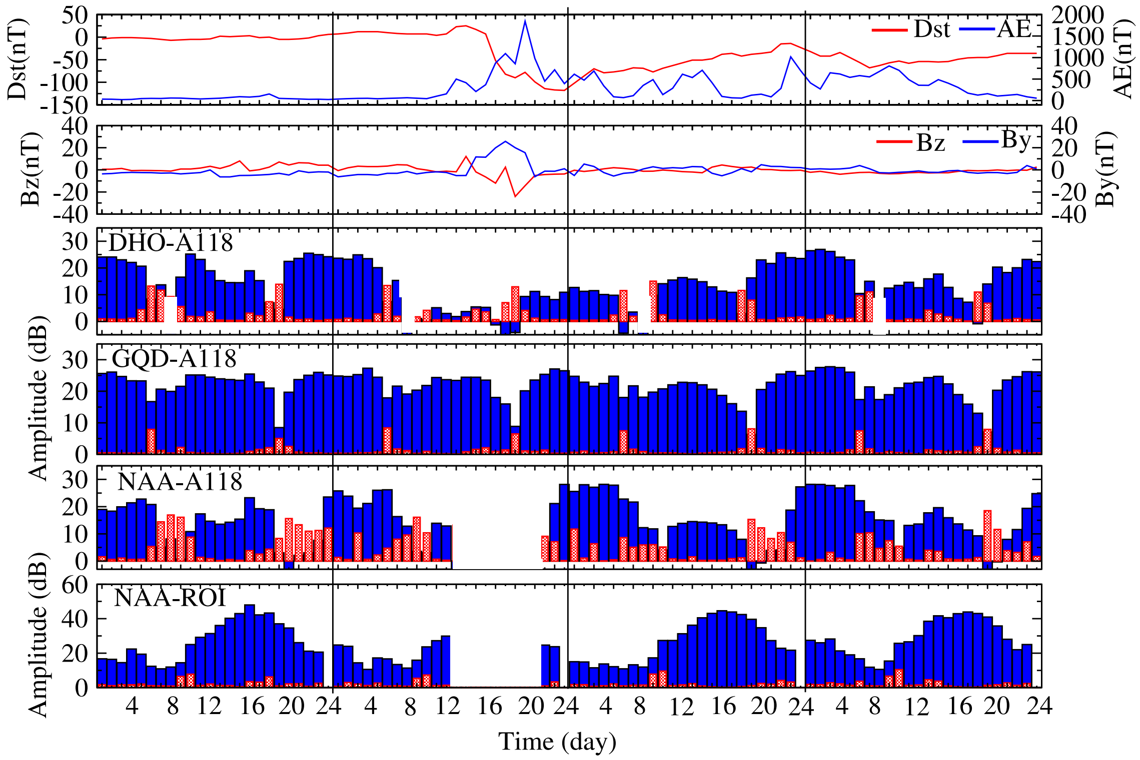

Figure 8. Variation in the MBSR, DTMA and the MASS for DHO-A118, GQD-A118, NAA-A118 and NAA-ROI propagation paths during 25-28 September 2011.

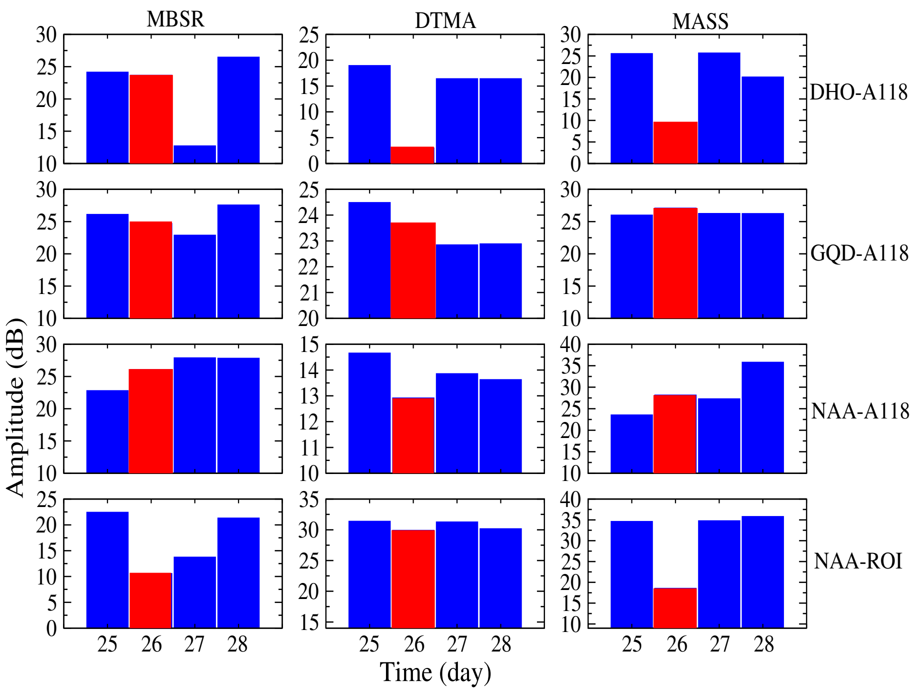

Figure 9. Variation in the MBSR, DTMA and the MASS for DHO-A118, GQD-A118, NAA-A118 and NAA-ROI propagations paths during 25-28 September 2011.

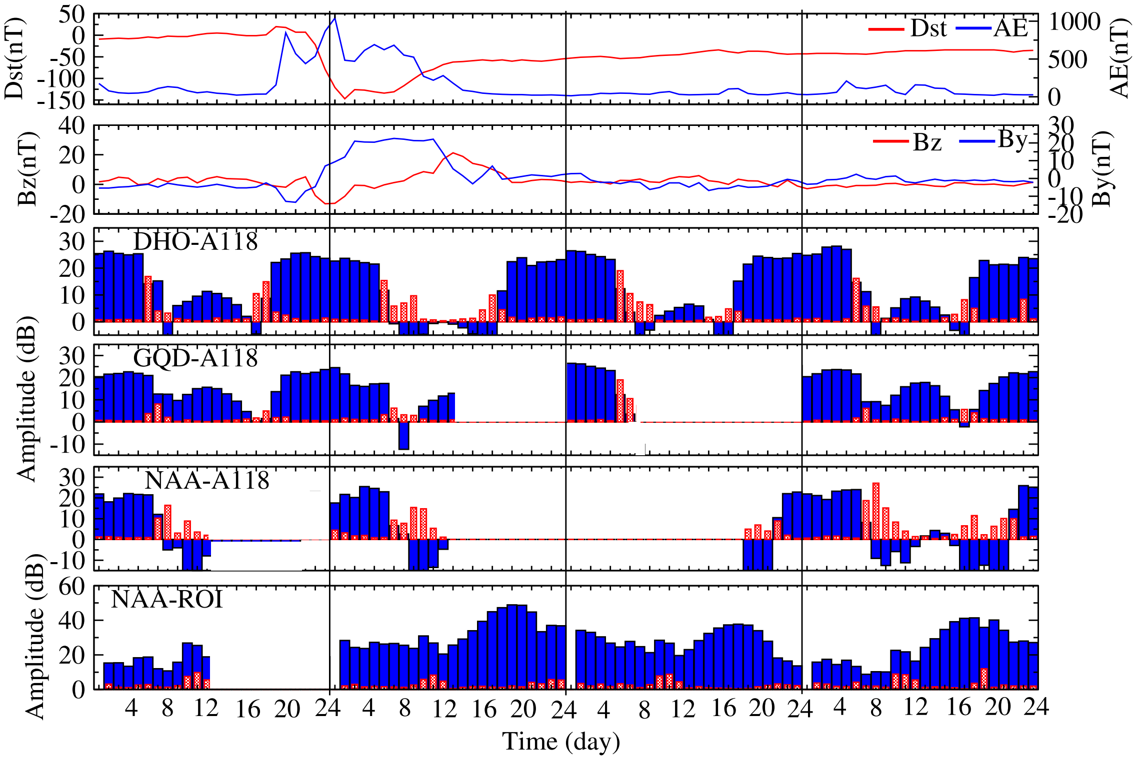

Figure 10. Variation in Dst, AE, B_y and B_z, and 1-hour averaged values of VLF amplitude for DHO-A118, GQD-A118, NAA-A118 and NAA-ROI propagation paths during 24-27 October 2011.

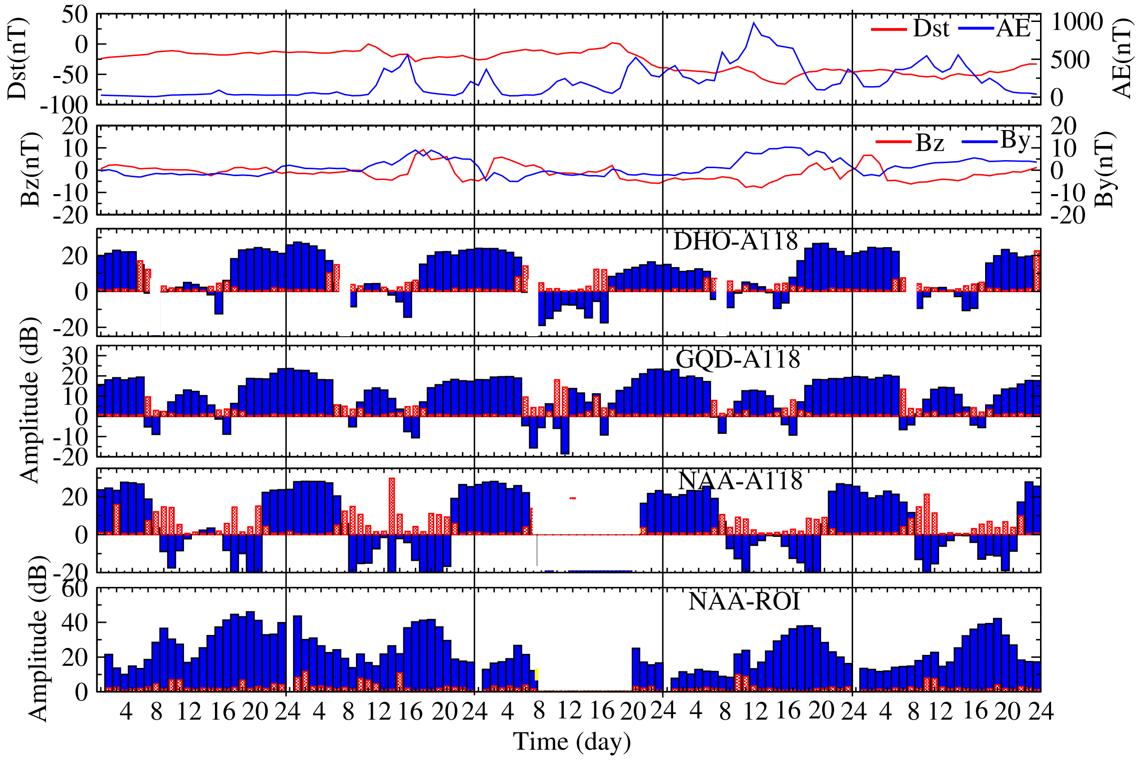

Figure 11. Variation in Dst, AE, B_y and B_z, and 1-hour averaged values of VLF amplitude for DHO-A118, GQD-A118, NAA-A118 and NAA-ROI propagation paths during 29-02 November 2011.

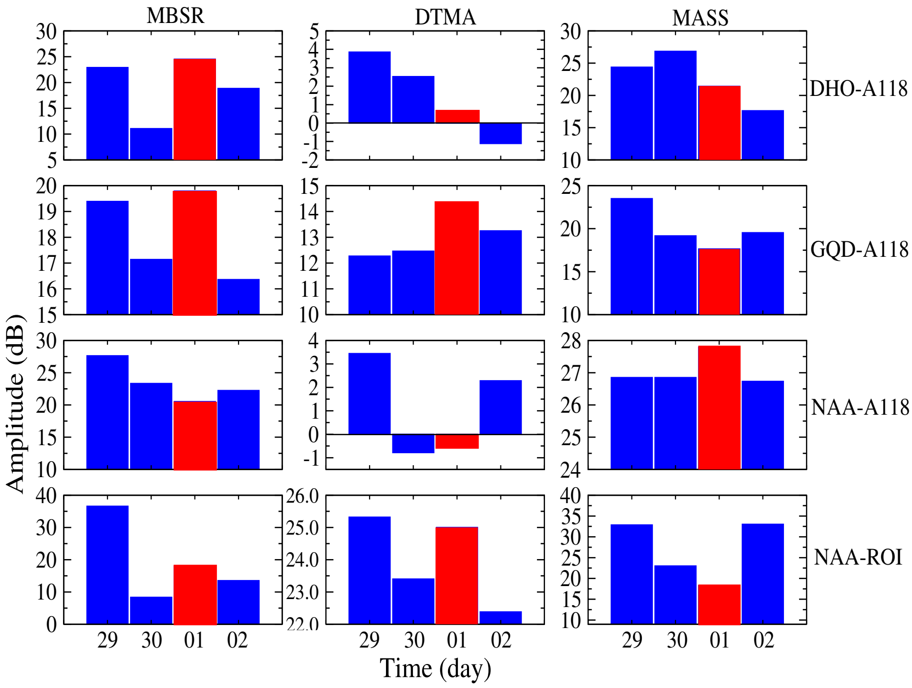

Figure 12. Variation in the MBSR, DTMA and the MASS for DHO-A118, GQD-A118, NAA-A118 and NAA-ROI propagation paths during 29-02 November 2011. Values for relatively quiet/undisturbed day (on 29 October) are contrasted with those of the storm day (on 1 November)

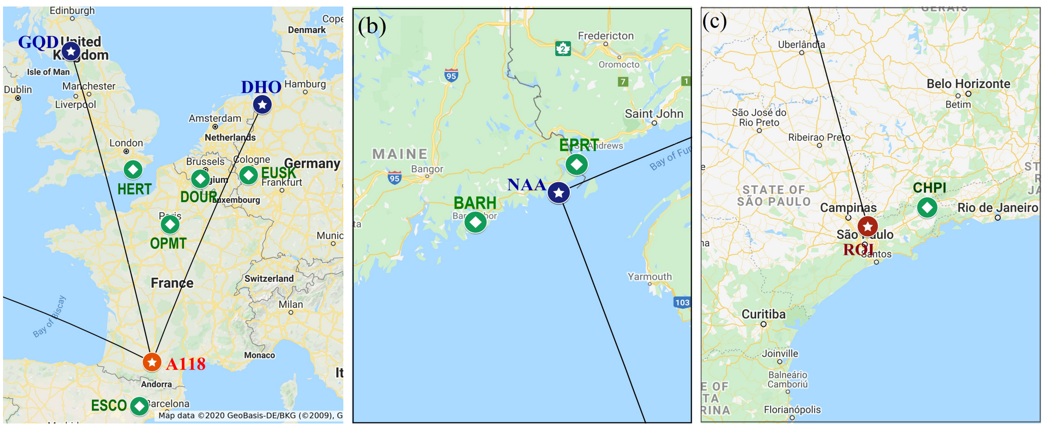

Figure 13. GNSS/TEC stations (green cicles) near/around the VLF transmitters, receivers and/or propagation paths.

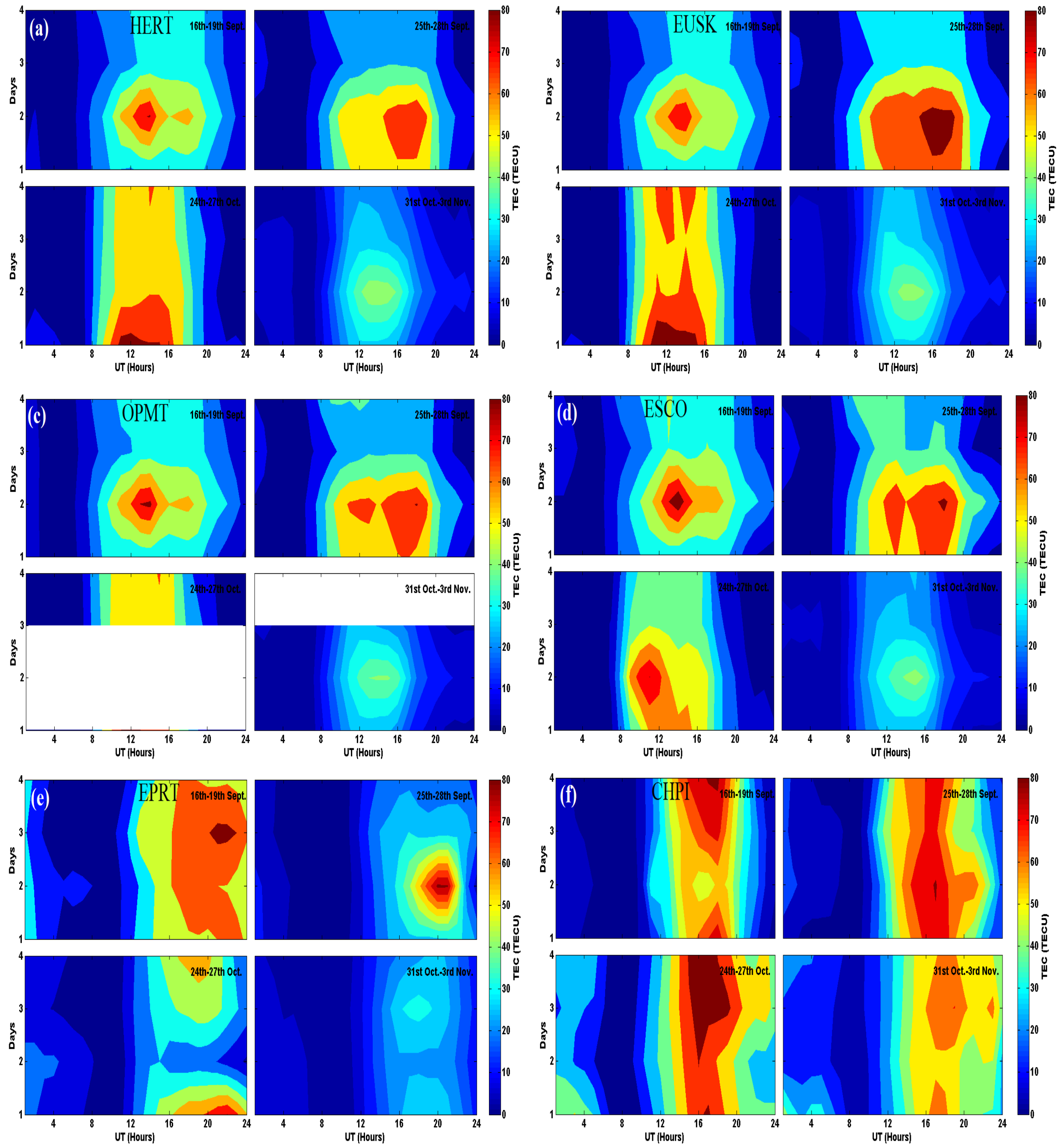

Figure 14. TEC contour plots for (a) HERT [Hailsham, UK] (b) EUSK [Euskirchen, Germany] (c) OPMT [Paris, France] (d) ESCO [Naut Aran, Spain] (e) EPRT [Eastport, United States] and (f) CHPI [Cachoeira Paulista, Brazil] Stations during 16-17 and 25-28 Septeber, 24-27 October and 31 October-03 November 2011.

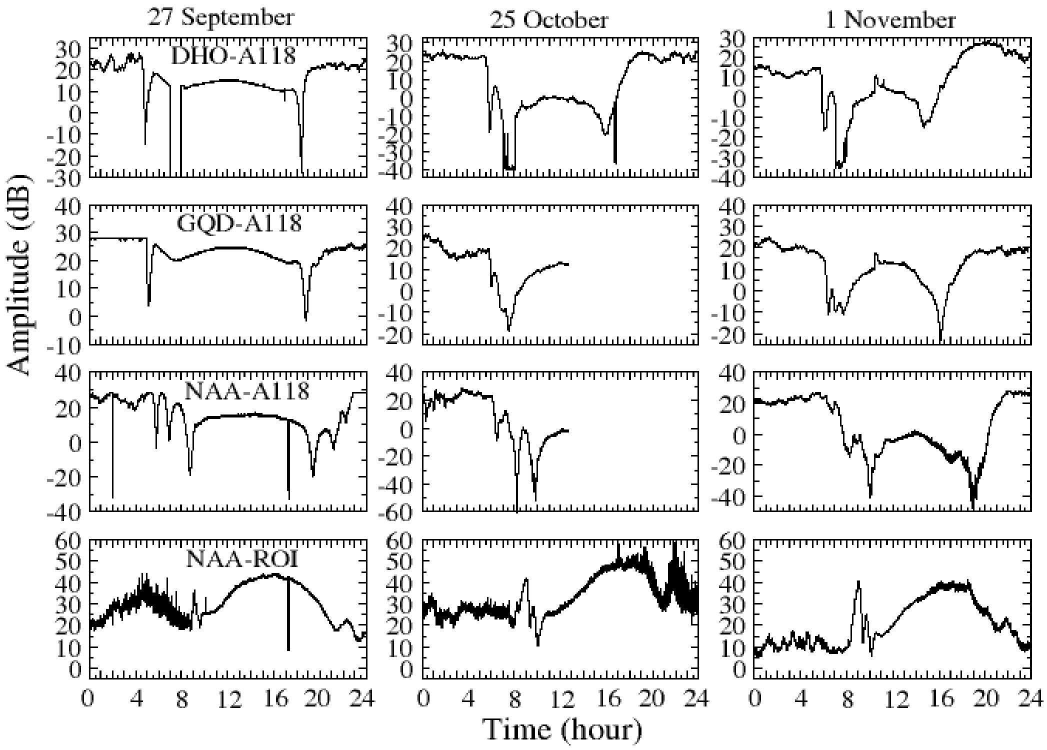

Figure 15. Anomalous signal observed in NAA-ROI propagation path during 27 September, 25 October and 1 Novenber 2011 geomagnetic storms.

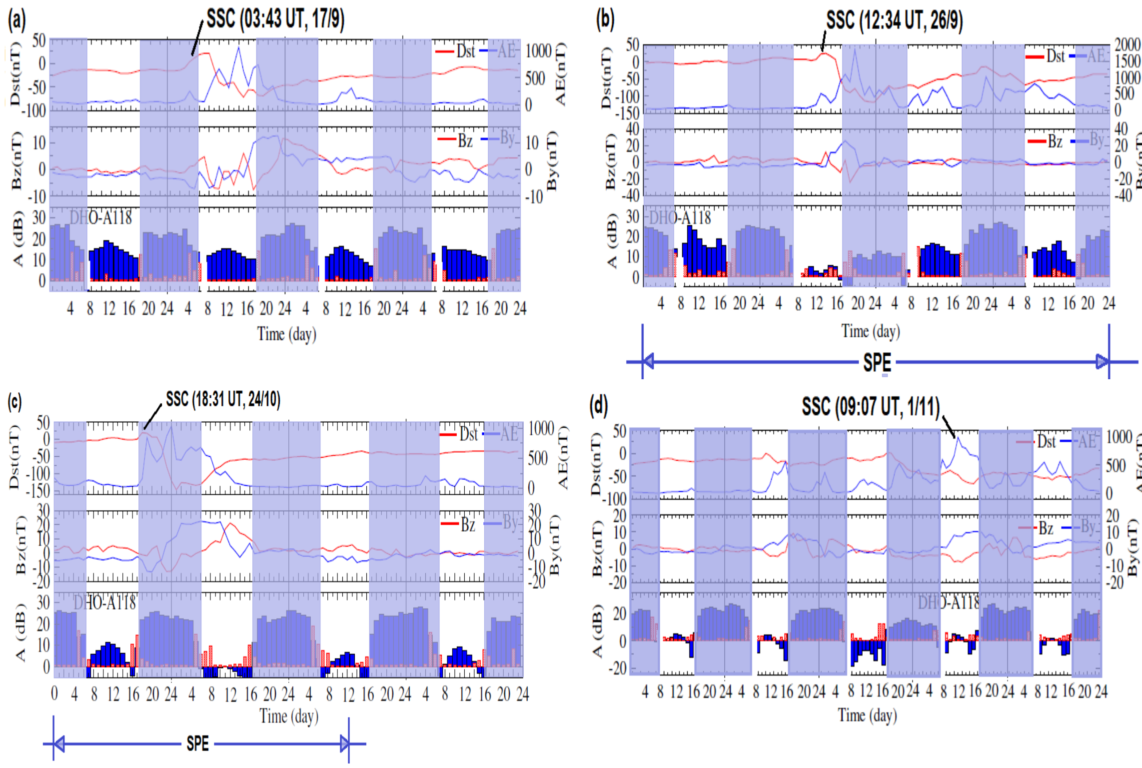

Figure 16. VLF amplitude data for the DHO-A118 emphasizing the 4 storm intervals during (a) 16-19 Septemebr (b) 25-28 September (c) 24-27 October and (d) 29 October - 02 November 2011.

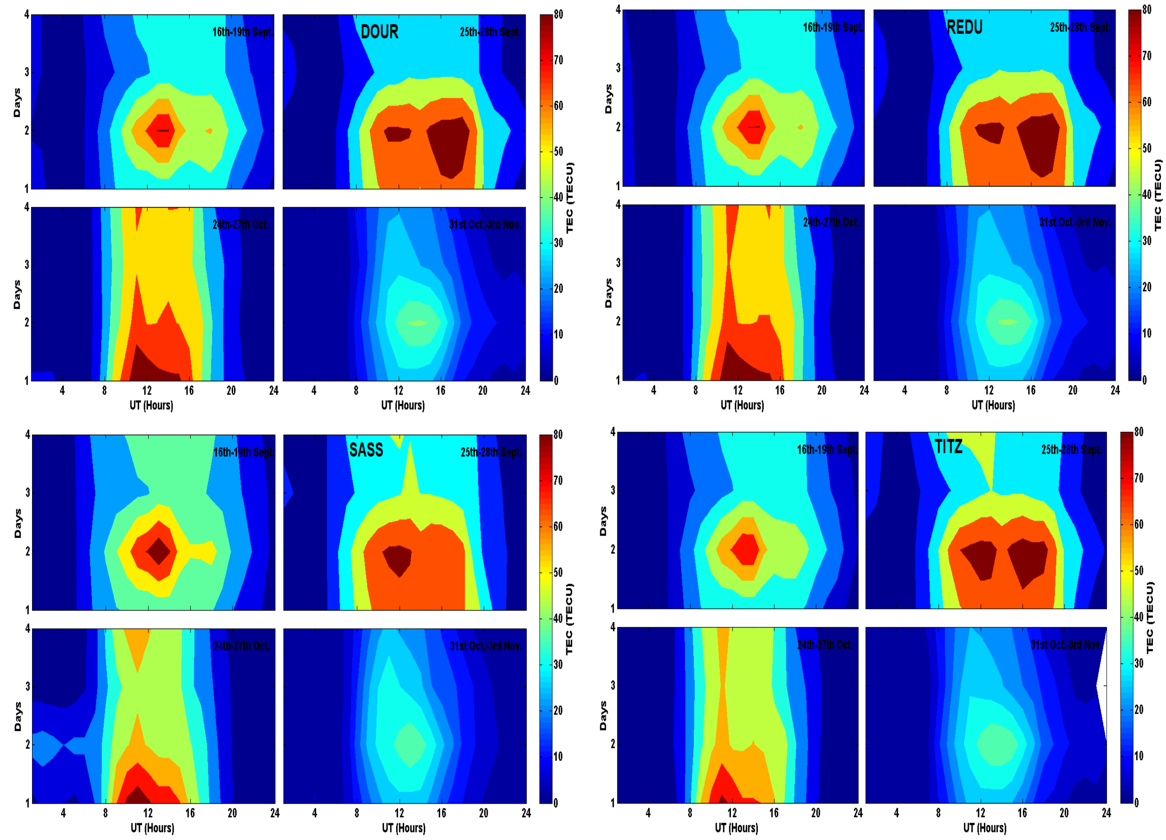

Figure 17. TEC contour plots for stations near the DHO-A118 propagation paths (REDU (Redu), DOUR (Dourbes), TITZ (Titz) and SASS (Sassnitz Island of Ruegen)) during the intervals 16-17 and 25-28 Septeber, 24-27 October and 31 October-03 November 2011.

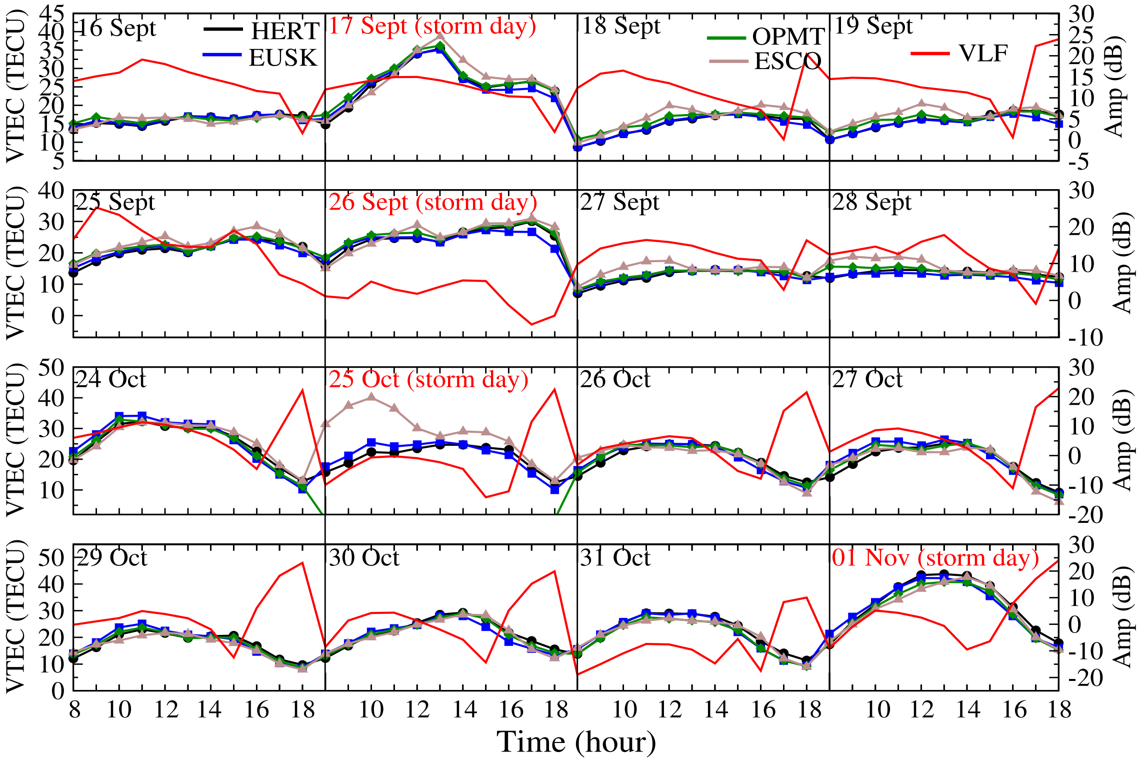

Figure 18. Daytime variation in VLF amplitude (red line plot) for DHO-A118 propagation path, together with VTEC values obtained from HERT (black line), EUSK (blue line), OPMT (green line) and ESCO (brown line) stations across Europe during 16-19 and 25-28 September, 24-27 October and 29 October-1 November 2011.